Hydration of gas-phase ytterbium ion complexes studied by experiment and theory

Philip X Rutkowski,[†] Maria C. Michelini,[‡,*] Travis H. Bray,[†] Nino Russo,[‡]

Joaquim Marçalo[§] and John K. Gibson[†,*]

[†]*Chemical Sciences Division, Lawrence Berkeley National Laboratory, Berkeley, CA 94720, USA*

[‡]*Dipartimento di Chimica, Università della Calabria, Via P. Bucci, Cubo 14 C, 87030 Arcavacata di Rende, Italy*

[§]*Unidade de Ciências Químicas e Radiofarmacêuticas, Instituto Tecnológico e Nuclear, 2686-953 Sacavém, Portugal*

* Corresponding authors: mc.michelini@unical.it (M.C.M); JKGibson@lbl.gov (J.K.G.)

Abstract

Hydration of ytterbium (III) halide/hydroxide ions produced by electrospray ionization was studied in a quadrupole ion trap mass spectrometer and by density functional theory (DFT). Gas phase YbX_2^+ and $YbX(OH)^+$ (X = OH, Cl, Br, or I) were found to coordinate from one to four water molecules, depending on the ion residence time in the trap. From the time-dependence of the hydration steps, relative reaction rates were obtained. It was determined that the second hydration was faster than both the first and third hydrations, and the fourth hydration was the slowest; this ordering reflects a combination of insufficient degrees of freedom for cooling the hot monohydrate ion, and decreasing binding energies with increasing hydration number. Hydration energetics and hydrate structures were computed using two approaches of DFT. The relativistic scalar ZORA approach was used with the PBE functional and all-electron TZ2P basis sets; the B3LYP functional was used with the Stuttgart Relativistic small core ANO/ECP basis sets. The parallel experimental and computational results illuminate fundamental aspects of hydration of f-element ion complexes. The experimental observations—kinetics and extent of hydration—are discussed in relationship to the computed structures and energetics of the hydrates. The absence of pentahydrates is in accord with the DFT results, which indicate that the lowest energy structures have the fifth water in the second shell.

Keywords: density functional theory; hydration; lanthanides; ytterbium halides; gas-phase reactions; kinetics

1. Introduction

The hydration of trivalent lanthanide cations and complexes in the condensed phase has been studied extensively. Experimentally, numerous studies have shown that the contraction of the lanthanide ionic radius across the series influences the number of water molecules coordinated to the bare trivalent cations. Most investigations report that, in aqueous solutions of lanthanide trihalides, the bare metal cations, Ln^{3+}, bond exclusively with water molecules and that halide anions are not in the first coordination sphere.[1-7] However, other studies have shown that direct metal-halide coordination can occur by altering the solution conditions. Steele and Wertz have demonstrated, using X-ray diffraction measurements, that $GdCl_2(H_2O)_6^+$ is an abundant complex in 10 N HCl solutions, whereas in more dilute aqueous solutions, the dominant species is $Gd(H_2O)_8^+$.[8] In a similar study, these authors, reported that $NdCl_2(H_2O)_6^+$ is an abundant species in a solution of $NdCl_3$ dissolved in (wet) methanol.[9] Using X-ray diffraction, Johansson and Yokoyama have shown that Cl and Br anions can enter the first coordination sphere of trivalent Er only in aqueous $ErCl_3$ and $ErBr_3$ solutions with high concentrations of the anion.[10]

Many theoretical studies have examined lanthanide ion hydration and coordination. A number of these studies applied molecular dynamics simulations of trivalent lanthanides in solution to understand the hydration of the bare metal cation.[11-15] Other studies focused on modeling trivalent lanthanide hydrates in the gas phase. A recent study by Kuta and Clark used DFT calculations to generate structures of the lanthanide hydrates with fully-hydrated first and second coordination spheres for the entire series.[16] Similar work has been done on gas-phase trivalent La[17] and Ce[18]. Another study by Clavaguéra, et al. modeled lanthanide trihalides and ion complexes.[19]

Knowledge of the nature of hydration of bare lanthanide ions and lanthanide complexes is necessary to understand geochemical processes. The solubility of lanthanides in brine solutions is especially important because the rare earth elements can be used as indicators to determine the mechanisms of hydrothermal ore deposition.[20] Geochemical studies focus on

temperature and pressure as a function of lanthanide halide solution speciation. A majority of these studies have concentrated on chloride-containing solutions, with only a few on fluoride solution speciation.[21] A study on dilute (~10^{-2} M) ytterbium (III) chloride solutions by Mayanovic, et al. showed that under high pressure and temperature (500 °C and 270 MPa), $YbCl_2^+\cdot(H_2O)_5$ is the predominant species.[22] Using X-ray absorption fine structure spectroscopy (XAFS), they determined that all five water molecules were directly coordinated to the Yb metal center. Mayanovic, et al. reported similar studies for trivalent Gd[23] and Nd[24] and found additional coordinated waters at high pressures and temperatures for the dichloride species: $GdCl_2^+\cdot(H_2O)_6$ and $NdCl_2^+\cdot(H_2O)_7$ respectively. Similarly, XAFS showed that all waters—remarkably up to seven in the latter case—were directly coordinated to the metal center. The decrease in terminal inner-sphere hydration, from seven for $NdCl_2^+$ to five for $YbCl_2^+$, can be attributed to the lanthanide contraction, which results in a decrease in the effective metal ion radius across the series.

We here report on the sequential hydration of trivalent biligated ytterbium dihalide, halide hydroxide, and dihydroxide cations, in the gas phase. A primary goal is to further understand the hydration of metal ion complexes, particularly of f-element metals, at a fundamental level by coupling experimental and theoretical studies of gas-phase hydrates and hydration. Electrospray ionization (ESI) was employed with quadrupole ion trap mass spectrometry (QIT-MS) to examine hydrated ions transferred from solution to the gas phase, as well as the relative kinetics of ion hydration in the gas phase. Of particular interest is the maximum degree of hydration which could be achieved in the gas phase under the most extreme accessible experimental conditions. Gas-phase hydrolysis was also observed. To understand the observed hydration behavior of these ions, computational methods were employed. The structures and energetics of the hydrates were computed and these results are compared with the experimental observations.

Ytterbium is a representative late lanthanide which exhibits a complex and distinctive isotopic pattern, allowing for definitive identification of Yb-containing species in mass spectra. A disadvantage of this isotopic complexity is that certain species cannot be effectively studied due to isobaric interferences; some studies were performed using the mono-isotopic neighboring lanthanide, Tm, which hydrates similarly to trivalent Yb. No experiments were performed on YbF_2^+ or $YbF(OH)^+$ due to the insolubility of YbF_3 in ESI solvents. Theoretical calculations

were carried out on YbX_2^+ and $YbX(OH)^+$ (X = OH, F, Cl), and their hydrates. A direct comparison between experiment and theory is possible for the chloride- and hydroxide-containing complexes; comparisons are extrapolated between computations and experiments for the bromide and iodide species.

2. Experimental Section

2.1 Materials. Solid $YbCl_3{\cdot}(H_2O)_6$, $YbBr_3{\cdot}(H_2O)_6$, $YbI_2{\cdot}(H_2O)_x$, and $TmCl_3{\cdot}(H_2O)_6$ were purchased from Sigma Aldrich and used without further purification. 100-350 μM solutions of the halide salts in isopropanol were prepared for ESI/MS experiments; no effort was made to maintain anhydrous isopropanol. The YbI_2 solutions were prepared using degassed isopropanol to prevent premature oxidation. Before injection into the electrospray capillary, the YbI_2 solutions were oxidized to form Yb(III) by a 50% dilution with non-degassed isopropanol/water (50/50). Partially deuterated isopropanol, $CH_3CHODCH_3$, and D_2O were used to elucidate the origins of hydroxides.

2.2 ESI/MS. All experiments were performed using an Agilent 6340 QIT-MS with MS^n Collision-Induced Dissociation (CID) capabilities. The instrument has a detection range of 50–2200 m/z, with a resolution of ~0.25 m/z. Mass spectra were recorded using the positive ion mode. Solutions were injected into an electrospray needle via a syringe pump and were nebulized using nitrogen gas upon exiting the needle, resulting in the creation of small droplets and eventually gaseous ions. The gas-phase cations entered a negatively-charged capillary where they were further desolvated by dry heated nitrogen from a liquid nitrogen dewar, which also supplied the nebulizing gas. Bare and hydrated cations passed through an ion-focusing skimmer and into two focusing octopoles for transfer into the ion trap. In the trap, specific ions were isolated by ejection of all other ions, enabling time-dependent hydration reaction studies. The temperature of the reactions in the ion trap is estimated to be ~298 K based on the work of Gronert.[25] The detailed instrumental parameters used for the ESI/QIT-MS experiments are in the Supporting Information. Pseudo-first order rate coefficients could not be determined in these experiments due to an unknown water pressure in the ion trap. Therefore, only relative reaction rates are reported. It is estimated, from similar experimental setups, that the water pressure in the ion trap was ~10^{-6} Torr.[26] Helium, present at ~10^{-4} Torr as the buffer gas in the trap, also served to collisionally cool the reactant ions prior to the start of kinetic measurements. Rates were determined by monitoring the decay of the reactant ion and ingrowth of the product ion(s)

as a function of reaction time; linear logarithmic decays of the reactant ions provided relative reaction rates. The helium provides third-body collisions which remove energy and stabilize hot product ions, which is crucial for adducts, such as hydrates. As discussed below, changes in the helium pressure substantially alter hydration rates, demonstrating that the product ions are cooled primarily by third-body collisions. Using the variational transition-state/classical trajectory theory of Su and Chesnavich, the collisional rate constants for all studied ions were found to be very similar (2.1 – 2.2 x 10^{-9} $cm^3 \cdot molecule^{-1} \cdot s^{-1}$).[27] This enables effective evaluations of relative hydration efficiencies by direct comparisons of reaction rates at a constant (unknown) water pressure; for these comparisons, relative reaction rates were normalized to the fastest reaction. The constancy of the water pressure in the trap was established by periodically confirming the invariance of the hydration rate for UO_2OH^+. Most of the relative rates for comparative purposes are considered uncertain by ±20%; a few values have larger uncertainties, as specified in the results tables.

3. Computational details

Two different approaches of DFT were used in these studies. The PBE functionals (exchange and correlation)[28,29] were used together with all electron triple zeta basis sets (TZ2P) as implemented in the ADF2007.01 software package.[30-32] Scalar relativistic corrections were included via the zero-order regular approximation (ZORA) in all ADF calculations (PBE–ZORA/TZP, hereafter). The numerical integration parameter in ADF was set to 6.0 for the optimizations and 8.0 for the frequencies. The increase in the numerical integration parameter with respect to the default values (4.0 for optimization and 6.0 for frequencies) did not significantly change the energies nor the geometries of the cations but helped to eliminate spurious imaginary frequencies lower than or close to 100 cm^{-1} present in systems containing water molecules in the second coordination shell.

Further calculations were done using the hybrid B3LYP[33,34] formulation together with the Stuttgart relativistic small core ANO/ECP basis set for the ytterbium atom (14s 13p 10d 8f 6g)/[6s 6p 5d 4f 3g].[35-37] This effective core potential replaces the 28 inner-shell electrons with a relativistically corrected pseudopotential. The 6-311++G(d,p) basis sets of Pople and co-workers[38-40] were employed for the rest of the atoms (B3LYP/SDD–ANO, hereafter). These calculations were carried out using the GAUSSIAN 2003 package.[41] “Ultra-fine” grids were adopted with the Gaussian program.

The levels of theory were chosen based on the performance observed in our previous studies of reactions containing heavy atoms,[42] and on recent theoretical studies of the hydration of Ln^{3+} cations.[16,18] However, at both levels of theory the choice of using larger basis sets was also based on some preliminary calculations performed on the bare cations, which showed an important dependence of the optimized geometries on the basis set sizes. In particular, the optimized structures of the bare cations performed using the double-zeta Stuttgart relativistic small core (12s 10p 8d 8f)/[5s 5p 4d 3f]) for the ytterbium atom together with the B3LYP functional differ substantially from the B3LYP/SDD−ANO results reported here, i.e. up to 35 degrees for the X-Yb-X/X-Yb-OH angles and 0.3 angstroms for the X-Yb/X-OH bond distances.

The sequential hydration reactions have been analyzed for five cations, namely, $Yb(OH)_2^+$, YbF_2^+, $YbF(OH)^+$, $YbCl_2^+$ and $YbCl(OH)^+$. The geometry of the bare and hydrated cations (one to six waters) was optimized without any symmetry restrictions at both PBE−ZORA/TZP and B3LYP/SDD−ANO levels, trying several initial geometries for each species. The lowest energy structures are reported for each cation along with some relevant high energy structures. In the case of the B3LYP/SDD−ANO calculations, the study was limited to the addition of up to three water molecules due to excessive computational demand using this approach. These computations provided enough information to perform a comparison between the results obtained at both levels of theory. Accordingly, the discussion is preferentially focused on the PBE−ZORA/TZP results and each section will present a comparison with the corresponding values obtained at the B3LYP/SDD−ANO level.

For each optimized stationary point, analytical frequencies were calculated in order to confirm that the optimized structures were local minima on the potential energy surface of the molecules, and to evaluate the zero-point vibrational energy (ZPVE) corrections to the electronic energies. All of the reported hydration energies include the ZPVE correction at 0 K (ΔE^0). In addition to the ΔE^0 values, the enthalpy (ΔH^{298}), entropy (ΔS^{298}), and Gibbs free energy (ΔG^{298}) changes are reported for each of the studied reactions. The accuracy of the ΔH^{298} and ΔS^{298} (and ΔG^{298}) values is necessarily somewhat limited by the use of the harmonic oscillator approximation to treat nuclear motion.

All of the studied cations have doublet spin states. Calculations were performed using spin−unrestricted methods and no spin contamination problems were found.

The charge distribution was analyzed using Natural Population Analysis (NPA)[43] and Atoms in Molecules (AIM)[44]. NPA was performed on the wavefunctions obtained at the B3LYP/SDD−ANO level of theory using Gaussian 2003, whereas AIM analysis was performed using ADF2009.01 on the ground state structures obtained at the PBE−ZORA/TZP level of theory. Molecular images were produced using Molekel4.3.[45]

4. Experimental Results

4.1 ESI/MS speciation. ESI mass spectra indicated the formation of gas-phase Yb(II) and Yb(III) cations with the chemical formulas: YbX^+, YbX_2^+ and $YbX(OH)^+$ (X = OH, Cl, Br, I). Additionally, hydrates of some of these species were also observed. Figures 1-3 show typical ESI mass spectra for solutions of $YbCl_3$, $YbBr_3$, and YbI_2 in isopropanol; the isopropanol, exposed to atmosphere, had absorbed an indeterminate amount of water. The top spectrum in each figure shows the cationic species formed by ESI, after transfer into the trap. Transfer and trapping of ions produced by ESI can result in extensive fragmentation, desolvation and/or reactions, such that these spectra are not representative of intrinsic ESI speciation. Additionally, an inherent delay occurs between when ions are accumulated in the trap to when they are ejected to the detector, during which ions may undergo hydration and/or hydrolysis by background water in the trap. To determine whether $YbCl(OH)^+$ and $Yb(OH)_2^+$ were produced during ESI or subsequently in the gas-phase, a deuterated solvent experiment was performed. ESI of a 350 μM solution of $YbCl_3$ in a 80/20 $CH_3CHODCH_3/D_2O$ mixture produced $YbCl(OH)^+$ and $Yb(OH)_2^+$, but negligible $YbCl(OD)^+$, $Yb(OH)(OD)^+$ or $Yb(OD)_2^+$. These results indicate that most hydrolysis does not occur during ESI but rather that $YbCl_2^+$ produced by ESI is hydrolyzed in the gas phase. As the hydrolysis rate of $YbCl_2^+$ in the ion trap is too slow to account for the observed amounts of $YbCl(OH)^+$ and $Yb(OH)_2^+$, hydroxide formation presumably occurs during ion transfer from the spray to the trap, where the background water pressure is much higher than in the trap.

Place Figures 1-3 Near Here

The YbX_2^+ and $YbX(OH)^+$ ions, and all four hydrates of each, were observed in the ESI mass spectra, except $YbBr_2^+$, YbI_2^+, and $YbI_2^+\cdot(H_2O)$. These ion complexes could have been absent because $YbBr_2^+\cdot(H_2O)$ and $YbI_2^+\cdot(H_2O)_2$ remain intact throughout the ESI and ion transport processes, which is consistent with the rationale below regarding stabilization of halide hydrates with low vibrational frequencies. The bottom spectra in Figures 1-3 show the ionic

species generated after a one second reaction time in the trap. Although bare $YbCl_2^+$ and its first three hydrates were not definitively observed in any mass spectra due to isotopic interferences (Figure 1, top), $YbCl_2^+\cdot(H_2O)_4$ was identified after hydration (Fig. 1, bottom), indicating the presence of bare and/or partially hydrated $YbCl_2^+$ in the parent mass spectrum.

4.2 Gas-phase hydration. The biligated Yb species and/or their hydrates, $YbX_2^+\cdot(H_2O)_n$ and $YbX(OH)^+\cdot(H_2O)_n$ (X = OH, Cl, Br, I; n = 0-3), hydrated in the gas phase. The gas-phase YbX_2^+ and $YbX(OH)^+$ species were hydrated by up to four waters, as demonstrated by allowing the ions to react with background water in the ion trap. A key observation was that hydration for all YbX_2^+ and $YbX(OH)^+$ species terminated at four coordinated waters under our experimental conditions; no pentahydrates were observed even with the maximum accessible reaction time of 10 seconds, as illustrated for $Yb(OH)_2^+$ in Figure 4. However, a very weak $Yb(OH)_2^+\cdot(H_2O)_5$ peak was observed with a relatively short reaction time of 200 ms, and an order of magnitude increase in water pressure in the ion trap by adding water to the trap through the helium gas inlet.

Place Figure 4 Near Here

The monoligated Yb species produced by ESI, YbX^+ (X = OH, Cl, Br, I), did not hydrate in the gas phase even using long reaction times. However, hydrates of YbI^+ were produced directly by ESI (Figure 3, top). Changes in the relative intensities of the $YbI^+\cdot(H_2O)_x$ peaks upon application of hydration delays indicated hydration of the hydrates. For example, the intensities of the $YbI^+\cdot(H_2O)_3$ and $YbI^+\cdot(H_2O)_4$ peaks relative to YbI^+, which did not hydrate, were respectively 4% and 0.3% in the ESI mass spectrum, and 17% and 15% after a one second hydration time.

4.3 Gas-phase hydration kinetics. Pseudo-first order hydration kinetics were determined from logarithmic decay plots, such as in Figures 5 and 6. Fewer than half of the isolated ions hydrolyzed in the gas phase, as discussed below. For the halide and hydroxide halide ions, gas-phase hydrolysis rates—i.e., replacement of a halide by a hydroxide upon reaction with water—were obtained from decay plots, such as in Figure 6; the hydrolysis contribution was then subtracted from the total reaction rate to determine the hydration rates. In most cases, no hydrolysis was observed and the hydration rate was the total reaction rate. In cases where hydrolysis and hydration of the isolated ion were the only reaction pathways, the total reaction rate was the sum of the two rates, e.g., the total reaction rate for $YbBr_2^+\cdot(H_2O)_2$ was the sum of the hydration rate, Eqn. (1), and the hydrolysis rate, Eqn. (2).

$$YbBr_2^+\cdot(H_2O)_2 + H_2O \rightarrow YbBr_2^+\cdot(H_2O)_3 \quad (1)$$

$$YbBr_2^+\cdot(H_2O)_2 + H_2O \rightarrow YbBr(OH)^+\cdot(H_2O)_2 \quad (2)$$

However, in a few instances, a produced-hydrate of the isolated ion also hydrolyzed and contributed to the total reaction rate. Using $YbBr_2^+\cdot(H_2O)$ as an example, the total reaction rate was the sum of the hydration rate, Eqn. (3), hydrolysis rate, Eqn. (4), and the hydrolysis rate of the produced-hydrate, Eqn. (2).

$$YbBr_2^+\cdot(H_2O) + H_2O \rightarrow YbBr_2^+\cdot(H_2O)_2 \quad (3)$$

$$YbBr_2^+\cdot(H_2O) + H_2O \rightarrow YbBr(OH)^+\cdot(H_2O) \quad (4)$$

In these instances, the reported hydration rates include the hydrolysis rate of the produced hydrate, i.e., the sum of the rates for Eqn. (3) and Eqn. (2), because the hydrolyzed hydrate is still a product of the hydration pathway. Because the water pressure in the trap was only estimated as ~10^{-6} Torr, kinetics are reported as absolute rates (i.e., s^{-1}), not as rate coefficients. Using the $UO_2(OH)^+$ hydration reaction for calibration and maintaining a constant helium pressure, it was confirmed that the water pressure was invariant to within <10% such that the measured hydration rates can be directly compared with one another. The intent here was not to measure rate coefficients, which depend on the cooling gas pressure, but rather to compare the relative rates of hydration.

Place Figures 5 and 6 Near Here

Due to experimental limitations—isotopic interferences and/or low ion intensities—hydration rates could not be effectively measured for several of the biligated ytterbium ions. In Table 1, the measured relative hydration rates are given. The hydration rates were normalized to the fastest measured hydration rate, which is the essentially identical second hydration rates of $Yb(OH)_2^+$ and $Tm(OH)_2^+$ as seen in Table 2; these normalized rates are shown in parentheses. A graphical representation of the measured rates as a function of hydration step is shown in Figure 7 to illustrate the trends in hydration kinetics. The relatively slow hydration of $Yb(OH)_2^+$ is evident in Figures 1-3: YbX_2^+ and $YbX(OH)^+$ are fully hydrated to the tetrahydrate after 1 s but $Yb(OH)_2^+$ is not; the comparative kinetics are discussed below.

Place Tables 1 and 2, and Figure 7 Near Here

To supplement the ytterbium results, thulium chloride was studied. Thulium, which is monoisotopic ^{169}Tm, is the lighter neighboring lanthanide to Yb such that the hydration rates of the corresponding ligated Tm(III) and Yb(III) ions should be very similar. The mass spectra for

the $TmCl_3$ solutions were similar to those for the $YbCl_3$ solutions, and similar hydrolysis was observed, as shown in Figure 8. The intensities of the peaks for $TmCl_2^+$ and its hydrates were very weak such that hydration rates could not be determined. The hydration rates for $Tm(OH)_2^+$, $TmCl(OH)^+$, and their hydrates were measured and were found to be similar to the Yb analogues—see Table 2. Given the close similarity between the rates for the first three hydrations of $Yb(OH)_2^+$ and $Tm(OH)_2^+$, the missing rate for the fourth hydration of $Yb(OH)_2^+$ is expected to be substantially slower than the other hydrations of $Yb(OH)_2^+$, perhaps roughly two orders of magnitude slower, as for $Tm(OH)_2^+\cdot(H_2O)_3$. Likewise, the undetermined rate for the third hydration of $YbCl(OH)^+$ is expected to be slower than the second, as for $TmCl(OH)^+$.

Place Figure 8 Near Here

The first and third hydration steps for biligated complexes generally exhibited similar rates whereas the second hydration step was relatively faster and the fourth was relatively slower. The first hydration of $YbBr(OH)^+$ was aberrantly slow. Referring to Figure 7, the following general ordering of hydration rates results from the measured kinetics: $1^{st} < 2^{nd} > 3^{rd} > 4^{th}$.

In the $TmCl_3$ experiments, TmO^+ was observed (Fig. 8), whereas from $YbCl_3$ no YbO^+ was observed (Fig.1). This difference is attributed to the propensity for Yb to exist in the divalent oxidation state, as in $YbOH^+$. Given this disparity between Yb and Tm, it should be emphasized that the experimental results reveal that hydration of the biligated trivalent Yb and Tm ions are similar: hydration is primarily an electrostatic interaction which does not involve a change in oxidation state.

4.4 Gas-phase hydrolysis. Hydrolysis was observed in the ESI experiments performed on ytterbium halide solutions. The $YbX(OH)^+$ and $Yb(OH)_2^+$ species were abundant in the parent ESI spectra from the halide solutions. As discussed above, the deuterium substitution experiments revealed that hydroxide formation occurs after ESI and before trapping, during ion desolvation and transport in the high-pressure regime of the instrument. In the X-ray diffraction studies previously mentioned, it has been demonstrated that hydrated Ln^{3+} ions, $Ln(H_2O)_{8,9}^{3+}$, not hydrolyzed lanthanides, $Ln(OH)_2^+$, are the abundant species in aqueous solutions under conditions such as those employed in this work.[8,9] The absence of $YbCl(OD)^+$ $Yb(OD)_2^+$ in the deuterium substitution experiments confirms that these hydroxides do not originate from solution, but rather form in the gas phase. Hydrolysis may occur in the ion trap when a reaction

time is applied—this was confirmed by results such as shown in Figure 6. All halide-containing ions hydrolyzed in the trap, with rates slower than for hydration: the hydrolysis reactions and rates are in Table 3. As discussed in the previous section, the total decay rate of the isolated ion is composed of the hydration rate, the hydrolysis rate, and, when applicable, the hydrolysis rate of produced-hydrates. The percentage of hydrolyzed species in the mass spectra of the isolated reactant was used to determine the hydrolysis rate as a fraction of the total reaction rate. The large difference between the hydrolysis rates for $TmCl(OH)^+$ (k = 1.0) and $YbCl(OH)^+$ (k = 3.2) is notable. The hydration rates for these two ions are very similar, as expected because the ion-water association interaction is essentially electrostatic. In contrast, the disparate hydrolysis rates evidently reflect different chemistries of the two ions. Another example of the differing chemistries of Yb and Tm comes from a study of D_2O reactions with gas-phase lanthanide cations where the primary reaction channel for Tm^+ was D_2O addition, whereas for Yb^+ OD-transfer was dominant.[46]

Place Table 3 Near Here

The relative intensities of the isotopically separated fully-hydrated biligated species after a one second hydration period (Figs. 1-3) provide an indication of the relative intensities of the dihalide, YbX_2^+, the partially hydrolyzed $YbX(OH)^+$, and the fully hydrolyzed $Yb(OH)_2^+$ produced during the period between ESI and trapping. Hydrolysis was most prevalent for the chloride and least for the iodide, as evident from the comparative abundances of the YbX_2^+ and $YbX(OH)^+$ hydrates in Figs. 1-3. After a one second hydration period, the relative intensities of the hydrates of $Yb(OH)_2^+$ / $YbX(OH)^+$ / YbX_2^+ were: 46% / 36% / 18% for X = Cl; 11% / 51% / 39% for X = Br; 7% / 38% / 55% for X = I.

5. Computational Results

5.1 Bare cation structures. Figures 9 to 13 show the optimized geometries of the YbX_2^+ and $YbX(OH)^+$ (X = OH, F, and Cl) bare cations as well as the lowest–energy structures of the successive hydrates. High energy structures are reported for some relevant penta– and hexa–hydrates. In the chemical formulas of the hydrates, water molecules in the second solvation shell are shown in italics.

Place Figures 9 – 13 Near Here

The bare halide/hydroxide ions exhibit folded structures with X–Yb–X and X–Yb–OH angles that vary between 105 and 116 degrees. Bond distances range from 1.91 Å (Yb–F) in YbF_2^+ to 2.40 Å (Yb–Cl) in $YbCl(OH)^+$ (PBE–ZORA/TZP). The B3LYP/SDD-ANO bond distances differ from the PBE-ZORA/TZP values by between 0.01 Å and 0.05 Å, and the largest difference found for angles is 11 degrees.

AIM analysis indicates that the atomic metal charges vary from 2.213 au in YbF_2^+ to 1.809 au in $YbCl_2^+$. The corresponding values obtained using the NPA approach are similar, with values of 2.392 au and 1.829 au, respectively. A comparison between the atomic charges obtained using the different methodologies shows that the largest difference is about 0.38 au. In general, greater positive metal charges are obtained using NPA on the B3LYP/SDD–ANO optimized wavefunctions. A complete report of the charge distribution for all of the ground state (GS) bare and hydrated cations is included in the Supporting Information (Tables S1 to S5).

5.2 Hydrate Structures. The addition of the first water molecule produces, in general, pyramidal structures with $Yb–OH_2$ distances that range between 2.28 Å in $YbF_2^+\cdot(H_2O)$ and 2.33 Å in $Yb(OH)_2^+\cdot(H_2O)$. The only exception is $YbF_2^+\cdot(H_2O)$, in which the GS has a planar geometry that is only slightly more stable than a pyramidal isomer (Relative Energy, RE = 12 $kJ\cdot mol^{-1}$) at the PBE–ZORA/TZP level of theory. In contrast, the B3LYP/SDD–ANO level of theory clearly favors the pyramidal structure. At this level, the planar structure (RE = 17 $kJ\cdot mol^{-1}$) is not a real minimum on the potential energy surface of the system (i 41 cm^{-1}). The addition of water induces a lengthening of the Yb–X (X = OH, F, Cl) bond, by between 0.01 Å and 0.06 Å, and an opening of the X–Yb–X or X–Yb–OH angle, by between 1 and 30 degrees.

The second hydration induces a further opening of the X–Yb–X or X–Yb–OH angle by no more than 5 degrees and a lengthening of the Yb–X distances by no more than 0.2 Å. The $Yb–OH_2$ distances are in general slightly longer (by up to 0.03 Å) than the corresponding length in the monohydrates.

The YbX_2^+ and $YbX(OH)^+$ cations in the trihydrates show linear structures with an exception of $YbF(OH)^+$, which is more distorted. The three water molecules are distributed fairly symmetrically, very close to a trigonal bipyramid structure. In the case of $YbF(OH)^+$, two other isomers were located at the PBE–ZORA/TZP level of theory, which are almost degenerate in energy (within 5 $kJ\cdot mol^{-1}$) and exhibit folded structures (Supporting Information, Figure S1).

The tetrahydrates are fairly symmetric with linear YbX_2^+ and $YbX(OH)^+$ structures. The GS geometries are slightly distorted from a bipyramidal structure. However, the $YbF(OH)^+$ cation presents a more distorted geometry. In general, similar to the previous hydrations, the addition of a fourth water molecule lengthens the bond distances of all of the ligands.

For all of the studied cations, the lowest energy pentahydrates are obtained when the fifth water molecule is placed in the second coordination shell. The fifth water forms two hydrogen bonds with two waters from the first coordination shell and a third hydrogen bond is formed only with the fluoride and hydroxide ligands.

Pentahydrated $YbX_2^+\cdot(H_2O)_5$ and $YbX(OH)^+\cdot(H_2O)_5$ isomers of the $YbX_2^+\cdot(H_2O)_4\textit{(H}_2\textit{O)}$ and $YbX(OH)^+\cdot(H_2O)_4\textit{(H}_2\textit{O)}$ GS structures were calculated to be, in all cases, between 3 and 20 $kJ\cdot mol^{-1}$ higher in energy (see Figs. 9 to 13). The addition of a fifth water molecule to the first coordination shell induces an expansion of the first shell with an average lengthening of the $Yb–OH_2$ bonds by 0.06 Å up to 0.1 Å.

The lowest energy hexahydrated complexes are characterized by the presence of four water molecules in the first coordination shell and two in the second shell. The coordination geometries are fairly symmetric with the second shell molecules forming two hydrogen bonds to different inner sphere water molecules and, when possible, a third hydrogen bond is formed with a fluoride or hydroxide ligand. No stable structures with six waters in the first coordination shell were located. However, structures with five waters in the first shell and a sixth in the second shell were located and determined to be high energy in all cases (see Figures 9 to 13).

Atomic charges calculated using AIM and NPA analyses for all of the bare and hydrated cations are summarized in tables S1 to S5 (Supporting Information). Both population analyses predict a decrease in the YbX_2^+ and $YbX(OH)^+$ charges resulting from a partial charge transfer from the first coordination shell of water molecules to the complex. The amount of charge transferred to the YbX_2^+ or $YbX(OH)^+$ unit after adding the first four water molecules ranged from 0.29 e^- for YbF_2^+ to 0.19 e^- for $Yb(OH)_2^+$. Therefore, the first solvation shell significantly stabilizes the charge of the cations through electron donation.

Clark and Kuta[16] have recently studied the trends in aqueous hydration of bare trivalent lanthanide cations and found that, in general, the addition of a second solvation shell induces a charge transfer from exterior to interior coordinated waters, which further decreases the charge on the metal by between 0.05 e^- and 0.16 e^-. In this same study, which used a level of theory

comparable to that used in this work, it was found that the NPA metal charge in $Yb(H_2O)_8^{3+}$ is 1.786 au; on average, each water molecule donates 0.13 e^- to the metal center. In the case of the YbX_2^+ and $YbX(OH)^+$ cations studied here, the addition of the second shell of water molecules generally increases the positive charge of the core unit because of the direct interaction established between the second shell water molecules and the X ligands. A more detailed discussion is included as Supporting Information.

5.3 Hydration energies. All of the studied biligated Yb cations are found to form stable hydrates. The reaction energies, enthalpies, entropies and Gibbs free energies for all six hydrations are summarized in Table 4. The reactions are in all cases exothermic and show a monotonic decrease with the increase in the number of coordinated waters.

Place Table 4 Near Here

The first and second hydration energies are very similar for $Yb(OH)_2^+$, $YbCl_2^+$ and $YbCl(OH)^+$, whereas the second hydration is less exothermic than the first hydration for YbF_2^+ and $YbF(OH)^+$ by about 20 kJ·mol^{-1}. For each of the studied cations, there is a substantial decrease in the exothermicity for the third hydration. That reduction ranges from 24 kJ·mol^{-1} for YbF_2^+ and $YbCl_2^+$ to almost 60 kJ·mol^{-1} for $Yb(OH)_2^+$. Such a precipitous decrease in binding energy from n = 2 to n = 3 has been observed previously for many transition metal ions, as recently summarized by Cheng et al.[46,47] : for example, the $Ti^+(H_2O)_n$ binding energies (in kJ·mol^{-1}) are 158±6 for n = 1; 136±5 for n = 2; and 69±7 for n = 3.

The energies of hydration of all tetrahydrates are quite similar, ranging from 78 to 86 kJ·mol^{-1}. The energies involved for the addition of a fifth water depends on the number of hydrogen bonds that are formed. When three hydrogen bonds are formed in a pentahydrate, which is the case for all of the cations except $YbCl_2^+$, the values range from 64 kJ·mol^{-1} to 70 kJ·mol^{-1}. However, in the case of $YbCl_2^+$, only two hydrogen bonds are formed and the exothermicity is only 60 kJ·mol^{-1}. The addition of the fifth water in the second shell requires energies that are between 10 kJ·mol^{-1} and 18 kJ·mol^{-1} lower in energy than the addition of the fourth water in the first shell. The only instance in which that difference is higher is for $YbCl_2^+$ (26 kJ·mol^{-1}), in which only two hydrogen bonds stabilize the fifth outer sphere water.

The formation of hexahydrates involves hydration energies that are similar to those of pentahydrates (within 8 kJ·mol^{-1}), provided that the addition of the fifth and sixth water

molecules involve the formation of an identical number of hydrogen bonds. For $YbCl(OH)^+$, the fifth hydration forms three hydrogen bonds and the sixth forms only two resulting in an energetic difference of about 20 $kJ\cdot mol^{-1}$.

A comparison between the energetic results obtained at the different levels of theory shows that the B3LYP/SDD–ANO level of theory gives hydration energies that are systematically between 7 $kJ\cdot mol^{-1}$ and 39 $kJ\cdot mol^{-1}$ more exothermic than those obtained using the PBE–ZORA/TZP approach. This difference is a combined effect of the different functional/basis sets and method (i.e., different ways of including the relativistic effects). As previously mentioned, there is also an important dependency of the optimized geometrical parameters with the size of the basis sets, which is particularly evident for the X-Yb-X and X-Yb-OH angles of the smallest systems (Section 3 and Figs. 9 to 13). Previous theoretical studies of the hydration of bare Ce^{3+} cations[18] have shown a very good agreement (within 3 $kJ\cdot mol^{-1}$) between gas-phase hydration energies when using PW91 (which is expected to behave similarly to the PBE functional used here) and B3LYP functionals, in combination with the same basis sets (double-zeta Stuttgart relativistic small core potentials). In the systems studied here, however, the hydration process also induces a weakening of the Yb-X and Yb-OH bonds, which is revealed by the lengthening of the corresponding bond distances (Figs. 9 to 13), which will also influence the calculated hydration energy and will probably be accounted for in a different manner by the different density functionals. Some test calculations performed at the B3LYP–ZORA/TZP level (single point calculations on the PBE–ZORA/TZP optimized structures of $Yb(OH)^+$ and its initial hydrates), do in fact give that are very close to the hydration energies calculated at B3LYP/SDD-ANO.

The entropy changes calculated for the first and second hydrations are similar. Those values range between -113 (-114) and -136 (-124) $J\cdot K^{-1}\cdot mol^{-1}$ for the first hydration at the PBE–ZORA/TZP (B3LYP/SDD-ANO) level of theory and between -100 (-117) and -132 (-135) $J\cdot K^{-1}\cdot mol^{-1}$ for the second hydration. There is an increase in the ΔS values for the third hydration with values between -126 (-132) and -156 (-145) $J\cdot K^{-1}\cdot mol^{-1}$ and a decrease for the fourth hydration with values between -112 and -124 $J\cdot K^{-1}\cdot mol^{-1}$. The addition of the fifth and sixth water molecules involves entropy changes that are much higher than those of the previous hydrations. Those values range between -154 and -180 $J\cdot K^{-1}\cdot mol^{-1}$ for the fifth hydration and between -164 and -181 $J\cdot K^{-1}\cdot mol^{-1}$ for the sixth hydration.

The hydration exoergicities, ΔG^{298}, are considered relevant to understanding the experimental observations and are included in Table 4. The trends are generally rather similar to those for the computed hydration energies and enthalpies, with a few exceptions. Among the more significant results is the value of ΔG^{298} for the third hydration of $Yb(OH)_2^+$, which is anomalously low at both levels of theory; it is notable that the corresponding ΔG^{298} for the third hydration of $YbX(OH)^+$ are also significantly lower than for the YbX_2^+ ions. Apparently, the hydroxide ligands destabilize the third hydrates in particular, due to both less favorable enthalpies and entropies.

6. Experimental Observations in Relation to Theory

6.1 Hydration kinetics. A central goal of this work is to explore the relationship between gas-phase hydration and computed hydration energetics and hydrate structures. Observed gas-phase hydration kinetics are determined by both thermodynamics—i.e., the driving force for the association reactions—and mechanistics—i.e., barriers to hydration, and/or dissociation of the nascent association complexes. Among the particularly intriguing aspects of the measured hydration kinetics is the observation that the first hydration step is invariably slower than the second (Fig. 7). The experiment and theory results can be directly compared for the particular cases of the first and second hydrations of $Yb(OH)_2^+$ and $YbCl(OH)^+$. For both of these species the second hydration is significantly more efficient than the first hydration (Table 1). Referring to the computed energetics for these hydrations (Table 4), the first hydration is more energetically favorable, as evaluated by both exothermicity (ΔH) and exoergicity (ΔG). Similar results—slower first addition than second addition—were reported and rationalized by Bohme and co-workers for NH_3 and D_2O association with bare metal cations.[48,49,47]

Association of a water molecule to a species such as $Yb(OH)_2^+$ should be essentially barrierless, with the water molecule binding to the exposed metal center, as in $Yb(OH)_2^+$ in Figure 9. Accordingly, the relatively inefficient first hydration is attributed to the efficient dissociation of the excited-state monohydrate, a process which is similarly barrierless. For the hydrate to survive, it must be cooled by third body collisions with the He bath gas before dissociation. To confirm collisional stabilization of association complexes under our experimental conditions, the He pressure dependence of the first hydration rate of $UO_2(OH)^+$ was examined at constant water pressure. The rate decreased by ~50% when the He pressure was halved, increased by ~30% when the He pressure was doubled, and decreased to ~2% in the

absence of He. The hot nascent hydrate complex is stabilized against prompt dissociation by dissipation of energy into internal modes of freedom, particularly vibrations: the greater and more accessible the vibrational degrees of freedom in the association complex, the greater the probability of its survival until collisional cooling. Our interpretation of the observed kinetics is that the first hydrates of $Yb(OH)_2^+$ (and the other biligated ions) are prone to promptly dissociate as compared with the second hydrates due to the lesser ligation and associated degrees of freedom for energy dissipation. This interpretation is consistent with the non-observation of hydration for the monoligated ions, YbX^+ (X = OH, Cl, Br, I) which possess fewer vibrational modes as compared with the biligated ions. The gas-phase hydration of the $YbI^+\cdot(H_2O)_{1\text{-}3}$ complexes produced by ESI is attributed to the degrees of freedom introduced by the coordinated water. In the NH_3 and D_2O association reactions mentioned above [47-49], the observation that the first associations were slower than the second for bare metal cations was similarly attributed to the fewer degrees of freedom for energy dissipation in the first association. It is intriguing that the first hydration of $YbBr(OH)^+$ is slower than that of both $YbCl(OH)^+$ and $YbI(OH)^+$. Such an apparent discontinuity down the halide series was not expected; however, analogously unique behavior of bromide has been reported in related systems. In particular, Anbalagan et al.[50] found that the CID behavior of $UO_2Br^+\cdot(H_2O)_3$ was very distinctive from that of $UO_2Cl^+\cdot(H_2O)_3$ and $UO_2I^+\cdot(H_2O)_3$.

The third hydration is slower than the second even though there are more vibrational degrees of freedom in the dihydrate than in the monohydrate complexes. The slower kinetics can be attributed to a large decrease in binding energy for the formation of the trihydrates. The calculated binding energies for all biligated Yb cations (Table 4) decrease considerably for the third hydration. A direct correlation between experimental and calculated results can be made for $Yb(OH)_2^+$ and $YbCl(OH)^+$; the reaction rates and binding energies for the third hydration decreased for both cations. In studies of NH_3 coordination reactions of Mg^+, Fe^+, and Ag^+ by Bohme and co-workers, the third association reactions also exhibited slower kinetics than the second association reactions; this trend was there attributed to the decrease in binding energies.[48,49]

The fourth hydrations of $Yb(OH)_2^+$ and $Tm(OH)_2^+$ (Figs. 1 and 9; Table 2) are very slow. As seen in Table 4, the energetics for this fourth hydration are quite favorable: the binding energies for the third and fourth waters, as indicated by both ΔH^{298} and ΔG^{298}, are comparable to

the third hydration within the accuracy of the computations. Furthermore, the presence of three coordinating waters in the reactant ion provides ample degrees of freedom to dissipate the hot hydrate prior to collisional cooling. Given the similar energetics for the third and fourth hydrations, the very slow kinetics for the latter can be attributed to greater steric crowding for the trihydrate as compared with the dihydrate (Fig. 9), which results in greater resistance to insertion of the fourth water.

The first hydration for $Yb(OH)_2^+$ is slower than for $YbCl(OH)^+$; the computed energetics for these hydrations, both ΔH^{298} and ΔG^{298}, are very similar. The computed vibrational frequencies for the $Yb(OH)_2^+$ and $YbCl(OH)^+$ bare cations are given in Table 5. The Yb–O stretching frequency for $YbCl(OH)^+$ was calculated as ~100 cm^{-1} lower than the same vibrational frequency for $Yb(OH)_2^+$. The Yb–Cl stretching frequency is much lower than the Yb–O stretch, by ~300 cm^{-1} in $YbCl(OH)^+$. The O–H stretching frequency was calculated to be much higher, at ~3800 cm^{-1} in both bare cations. The lower frequency Yb–Cl stretch would allow the bare $YbCl(OH)^+$ to dissipate the energy of hydration more efficiently in the vibrational modes of the "floppy" Yb-Cl bond, resulting in a faster hydration rate as compared with $Yb(OH)_2^+$ due to stabilization of the nascent hot hydrate by internal dissipation of the excess energy.

6.2 Absence of pentahydrates. Calculations show that the heats of formation for the pentahydrate Yb complexes are exothermic. The experimental results for the first four hydrates have been primarily evaluated in the context of the computed energies (enthalpies) of hydration; for these hydrates, the computed ΔG^{298} values are less favorable due to the positive entropy of association, but predict the observed hydration. A key issue is whether the exothermicity, ΔH^{298}, or the exoergicity, ΔG^{298}, should be considered in the evaluation of gas-phase reactions.[51] At very low pressures (e.g., $<10^{-6}$ Torr) where third body collisions are rare and reactions are bimolecular, the role of entropy is uncertain, particularly as it is problematic to define the "temperature" of such an isolated reaction system. At higher pressures, such as ~10^{-4} Torr in the experiments reported here, it is clear that third body collisions are crucial to stabilize the hydration product, such that the concepts of temperature (i.e., $T \approx 298$ K), entropy, and Gibbs free energy are more clearly relevant. The demonstration of the formation of a pentahydrate at relatively high water pressure—but not for long reaction times at lower pressure—suggests an approach to equilibrium conditions, and thus the necessity for consideration of ΔG^{298}.

It is seen from the values in Table 4 that whereas the ΔH^{298} values decrease only modestly between the fourth and fifth hydration, the ΔG^{298} values for the fifth hydrations become substantially less favorable than for the first four hydrations, which may explain the absence of pentahydrates under our standard experimental conditions: no pentahydrate species were detected in mass spectra with the background water pressure despite that ΔG^{298} is favorable, albeit by only ~20 $kJ \cdot mol^{-1}$. Calculations also show that, for all complexes, the lowest energy pentahydrate geometries contain four waters in the first coordination shell and one water in the second coordination shell. Following the logic of Bohme and co-workers [47], the distinct decrease in binding of the fifth waters can be attributed to "a change in the nature of the bonding from direct bonding to hydrogen bonding in a second coordination shell". The water pressure in the ion trap is evidently adequately low to favor dehydration over second-shell hydration. A hydrated monopositive ion which undergoes second-shell hydration is somewhat similar to addition of water to a microdroplet in the gas phase; the positive charge and the ordered orientation of the inner-sphere waters distort from this simplistic scenario, but the very large decrease in ΔG^{298} between the four inner-sphere and the fifth and sixth outer-sphere hydrations (Table 4) is consistent with this picture. At a water pressure of ~10^{-6} Torr and a temperature of 298 K, growth of water droplets, even nanodroplets, is unfavorable. It is feasible that inefficiently formed inner-shell pentahydrates might be observed at reaction times longer than 10 s.

A minor amount of the pentahydrate of $Yb(OH)_2^+$ was seen when the water pressure in the ion trap was increased by an order of magnitude, with a reaction time of 200 ms. In contrast, increasing the reaction time by an order of magnitude does not produce the pentahydrate. This is in accord with the proposition that it is the equilibrium in Eqn. (5) which determines whether or not this outer-shell fifth hydrate is observed.

$$Yb(OH)_2^+ \cdot (H_2O)_4 + H_2O \leftrightarrow Yb(OH)_2^+ \cdot (H_2O)_4 \textit{(H_2O)} \qquad (5)$$

7. Conclusions

Hydration for the gas-phase YbX_2^+ and $YbX(OH)^+$ (X = OH, Cl, Br, I) cations terminated at four waters. No pentahydrate complexes were observed, except for a $Yb(OH)_2^+$ pentahydrate detected only with an order of magnitude increase in water pressure in the ion trap. DFT calculations show that the formation of YbX_2^+ and $YbX(OH)^+$ hydrates (X = OH, F, Cl) are all exothermic; computations were performed for monohydrates to hexahydrates. The calculations

indicate that for the cations studied, pentahydrates with four inner-shell waters and one outer-shell water are energetically more favorable than pentahydrates with five inner-shell waters. The absence of outer-sphere pentahydrates is in accord with previous studies by Bohme and co-workers [47-49], and can be attributed to rapid dehydration of the outer-sphere water and a steric hindrance to addition of a fifth inner-shell water.

Hydration kinetics were determined by isolating selected ions and allowing reactions with ~10^{-6} Torr water in the ion trap for variable times. The general ordering of hydration rates for the biligated cations was $1^{st} < 2^{nd} > 3^{rd} > 4^{th}$ ($>> 5^{th}$). The computed energetics do not account for this ordering and we invoke the rationale put forth by Bohme and co-workers [47-49]: the first hydration is inefficient due to fragmentation of the hot association complex with few degrees of freedom; the efficiencies of subsequent hydrations are dominated by the binding energies; the great inefficiency of the fifth hydration reflects a shift to outer-shell coordination.

Acknowledgments

This work was supported by the Director, Office of Science, Office of Basic Energy Sciences, Division of Chemical Sciences, Geosciences and Biosciences of the U.S. Department of Energy at LBNL, under Contract No. DE-AC02-05CH11231; by the Universitá della Calabria. M.C.M. is grateful for the opportunity to be a Guest Scientist in the Chemical Sciences Division at LBNL. J.M. is indebted to the Chemical Sciences Division of LBNL for the opportunity to visit the Berkeley lab in the summer of 2009. The CINECA supercomputing centre (Casalecchio di Reno, Italy) is acknowledged for the computational time.

Supporting Information

Instrumental parameters for the ESI/QIT-MS experiments. Complete citation for reference 21. NPA and AIM charge analyses for all of the bare and hydrated YbX_2^+ and $YbX(OH)^+$ cations (GS structures). Alternative $YbF(OH)^+\cdot(H_2O)_3$ structures (PBE-ZORA/TZP level of theory).

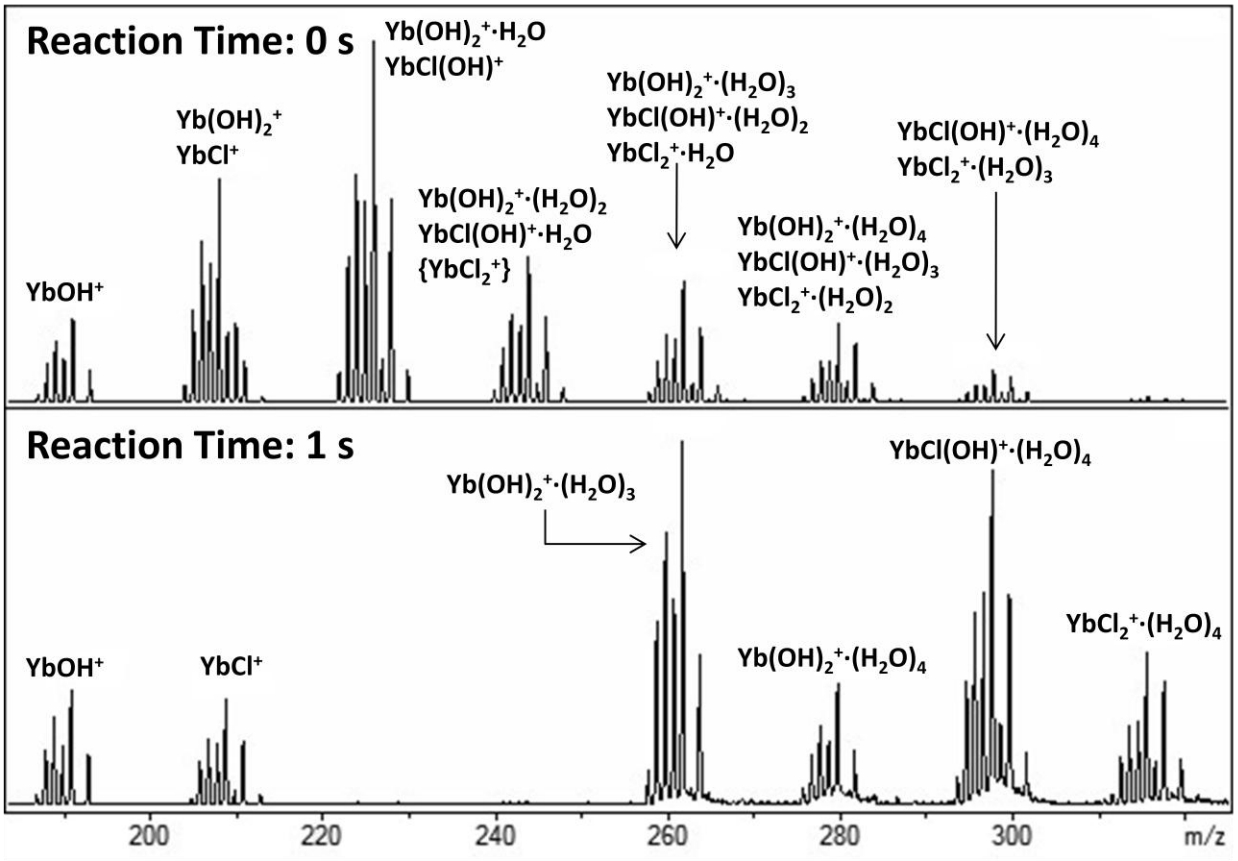

Figure 1. ESI/MS of $YbCl_3$ in isopropanol. The top spectrum is from ESI/MS. The bottom spectrum shows the gas-phase speciation after a one second reaction period in the trap. The $YbCl_2^+$ species in brackets was not definitively identified.

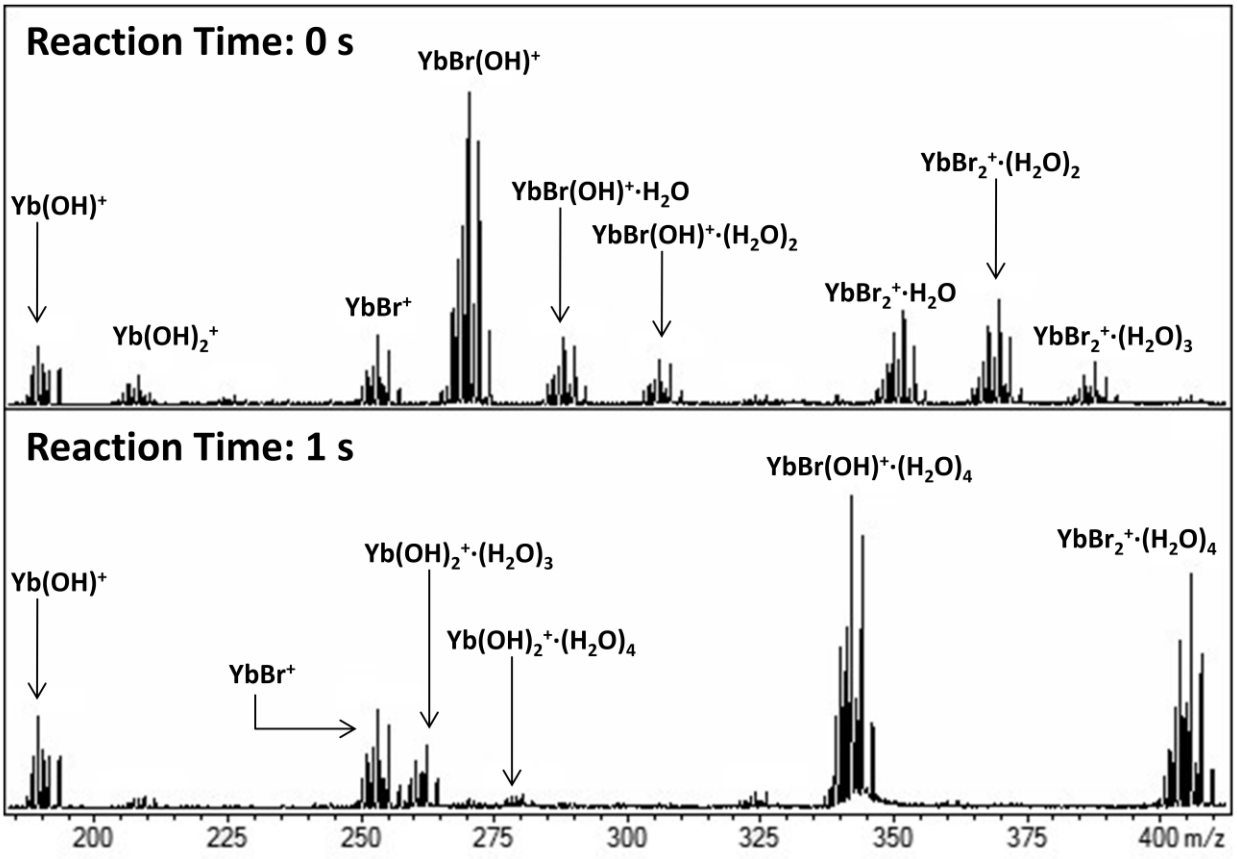

Figure 2. ESI/MS of $YbBr_3$ in isopropanol. The top spectrum is from ESI/MS. The bottom spectrum shows the gas-phase speciation after a one second reaction period in the trap.

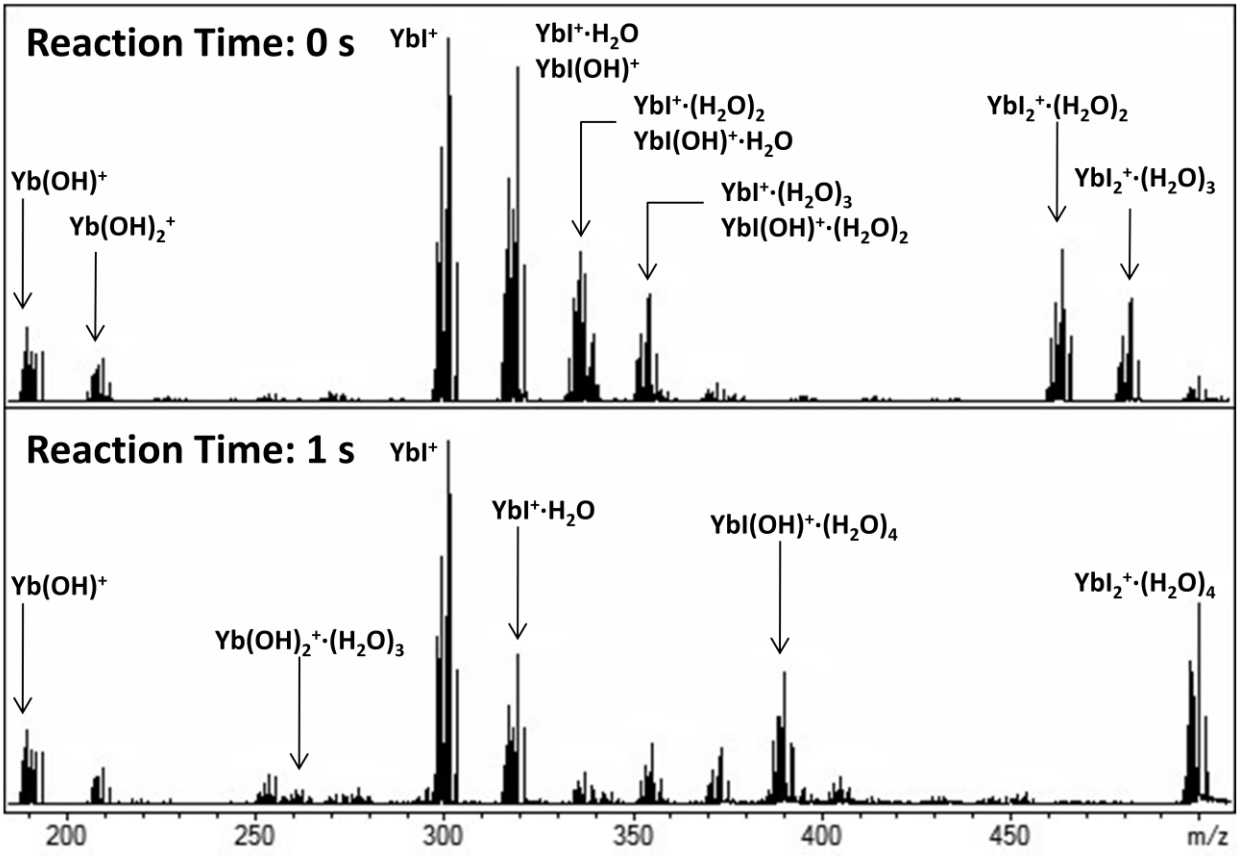

Figure 3. ESI/MS of YbI_2 in isopropanol. The top spectrum is from ESI/MS. The bottom spectrum shows the gas-phase speciation after a one second reaction period in the trap.

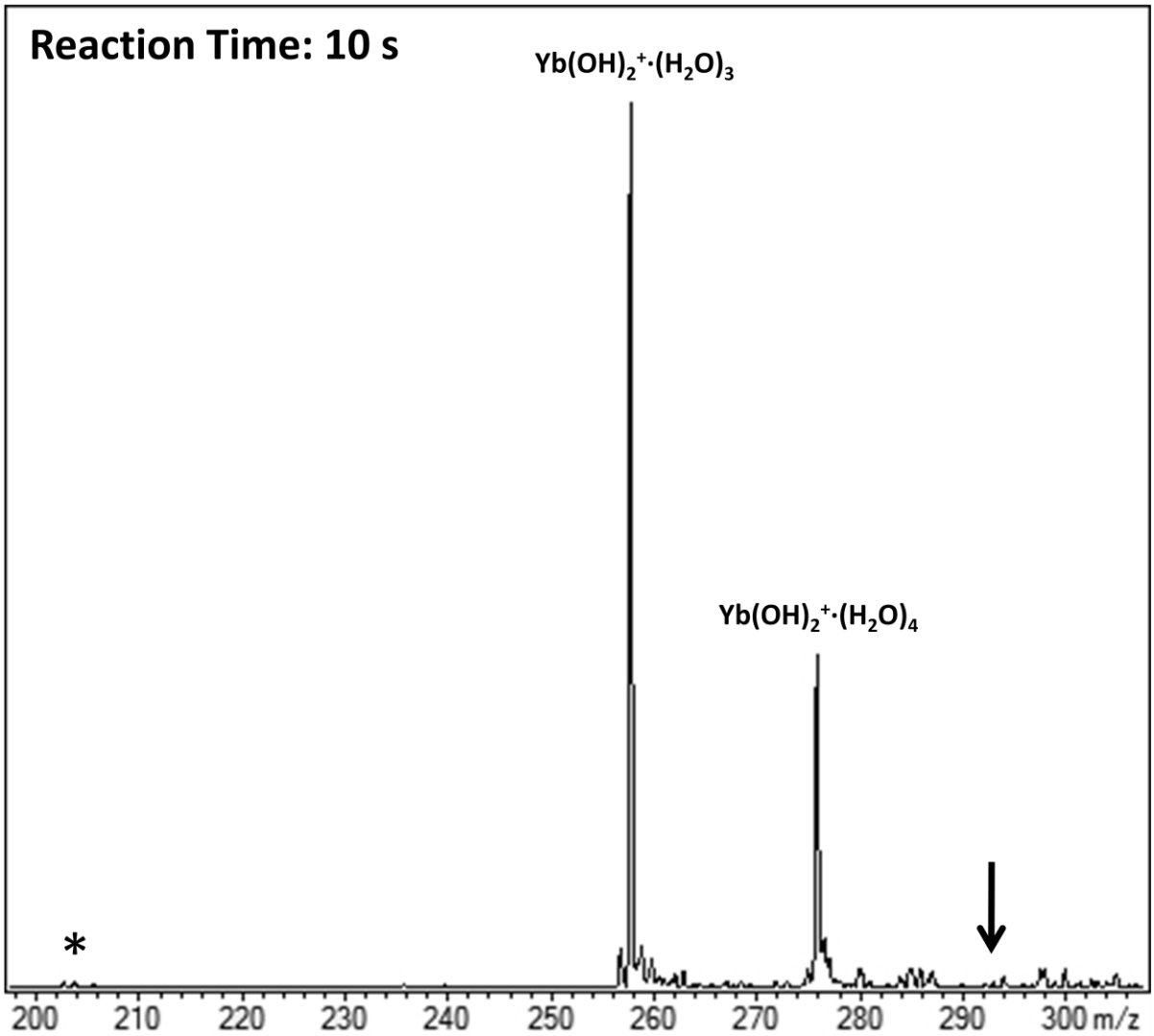

Figure 4. Isolated $Yb(OH)_2^+$ with a 10 second reaction time. The asterisk represents the location of the isolated ion. The arrow indicates where the pentahydrate would appear.

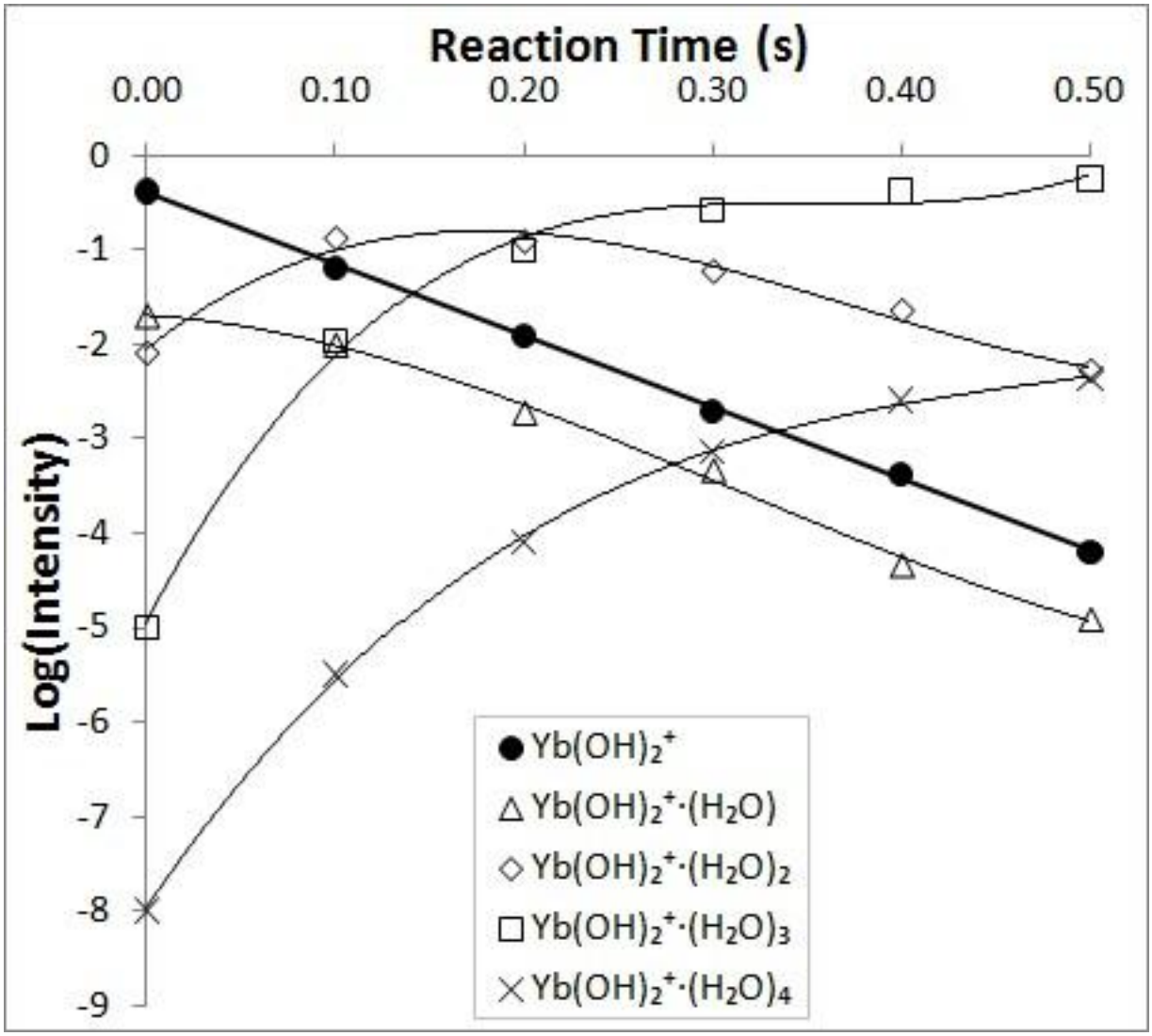

Figure 5. Time profile of $Yb(OH)_2^+$ hydration. $Yb(OH)_2^+$ ions produced from ESI of solutions of $YbCl_3$ in isopropanol were isolated and hydrated by water in the ion trap. The linear decay provides the hydration rate for $Yb(OH)_2^+$.

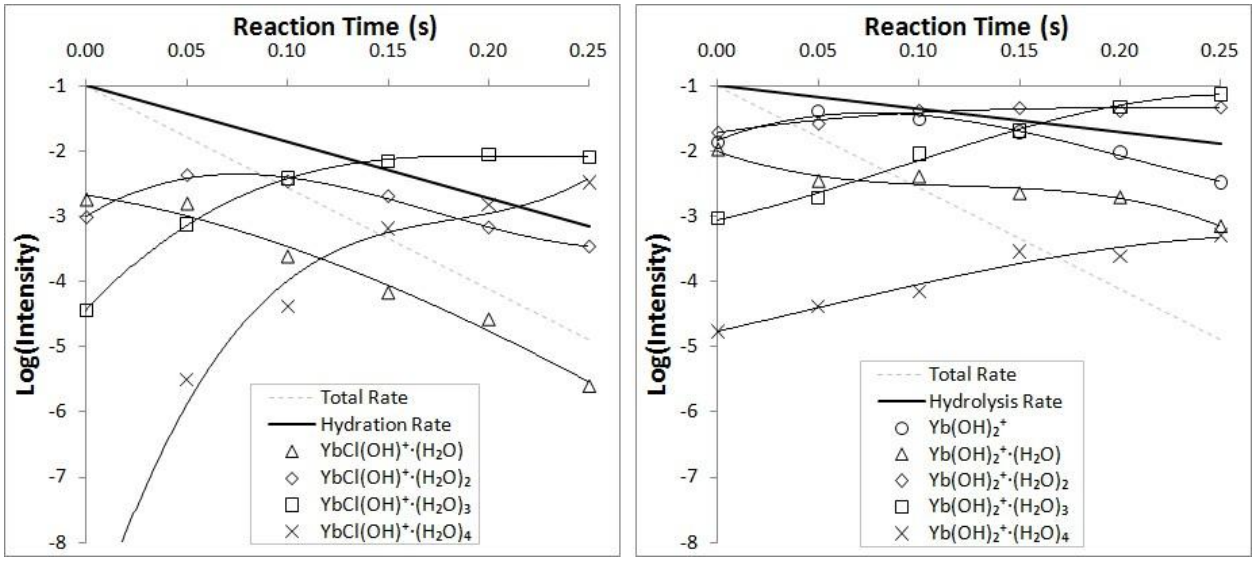

Figure 6. Time profile of $YbCl(OH)^+$ hydration (left) and hydrolysis (right). $YbCl(OH)^+$ ions were produced from ESI of $YbCl_3$ in isopropanol. $YbCl(OH)^+$ ions were isolated and hydrated or hydrolyzed by water in the ion trap. Hydration and hydrolysis kinetics were determined by altering the reaction time in the ion trap.

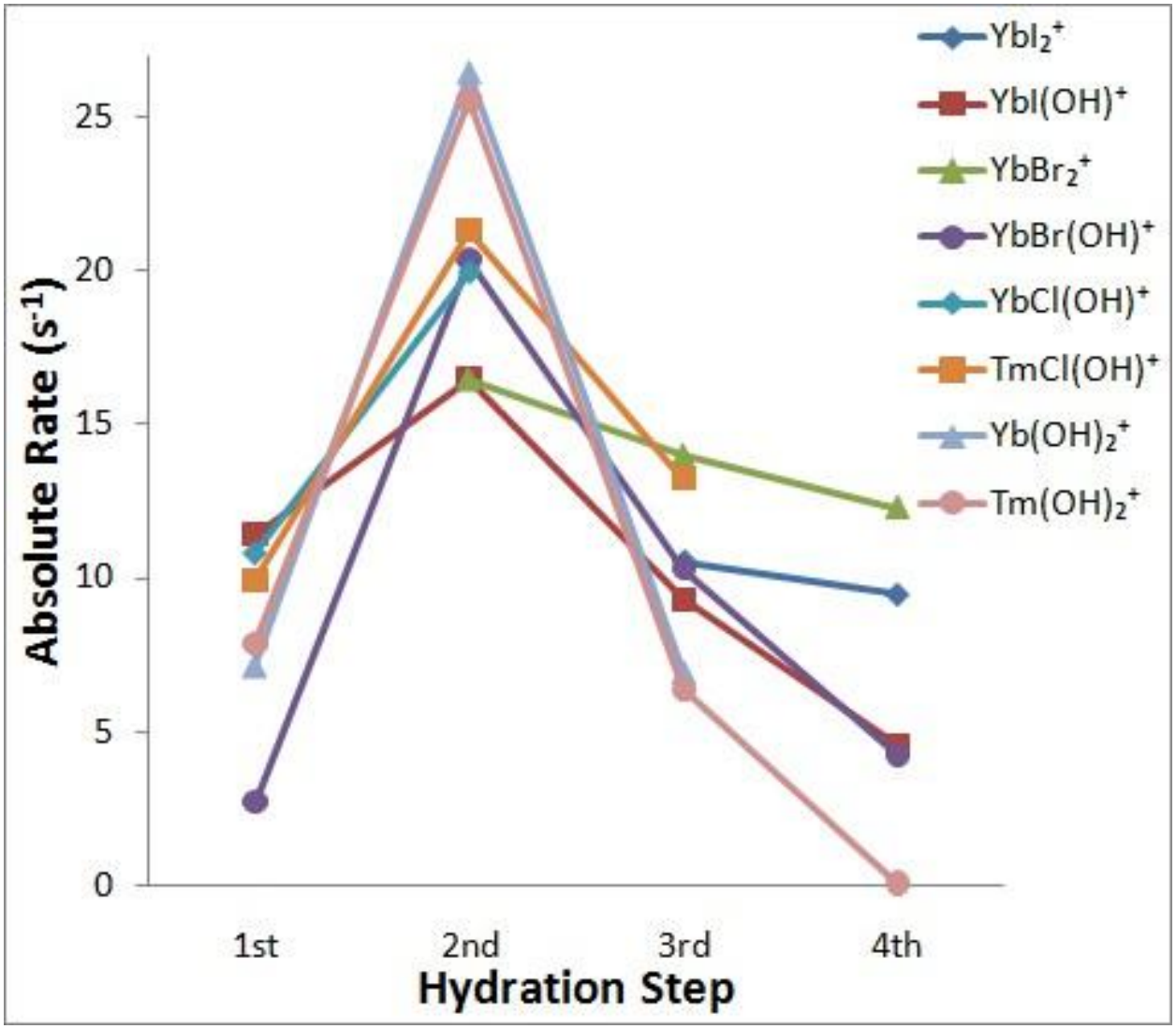

Figure 7. Absolute hydration rates plotted as a function of hydration step. The second hydration for all studied ion complexes was the fastest; the fourth hydration was the slowest.

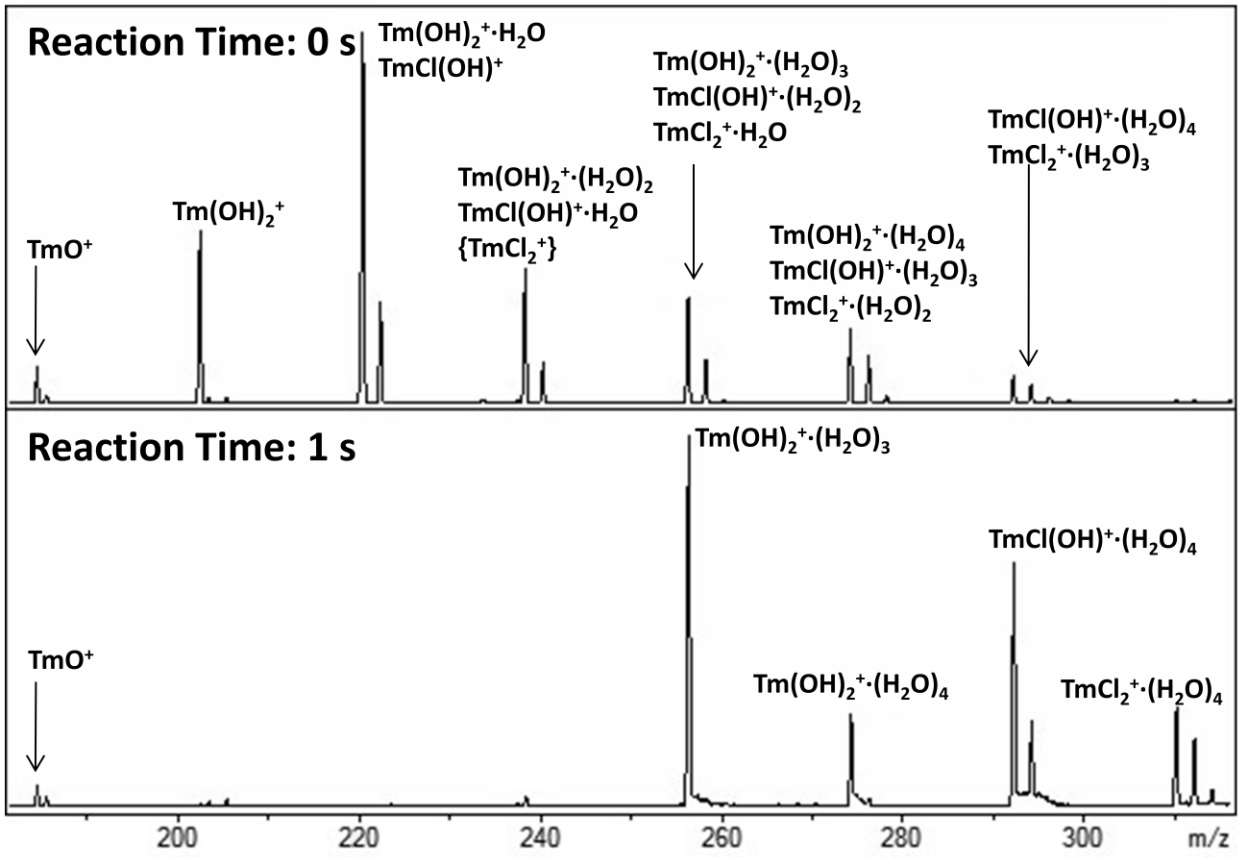

Figure 8. ESI/MS of $TmCl_3$ in isopropanol. The top spectrum is the ESI/MS. The bottom spectrum shows the gas-phase speciation after a one-second reaction period in the trap. The $TmCl_2^+$ species in brackets was not definitively identified.

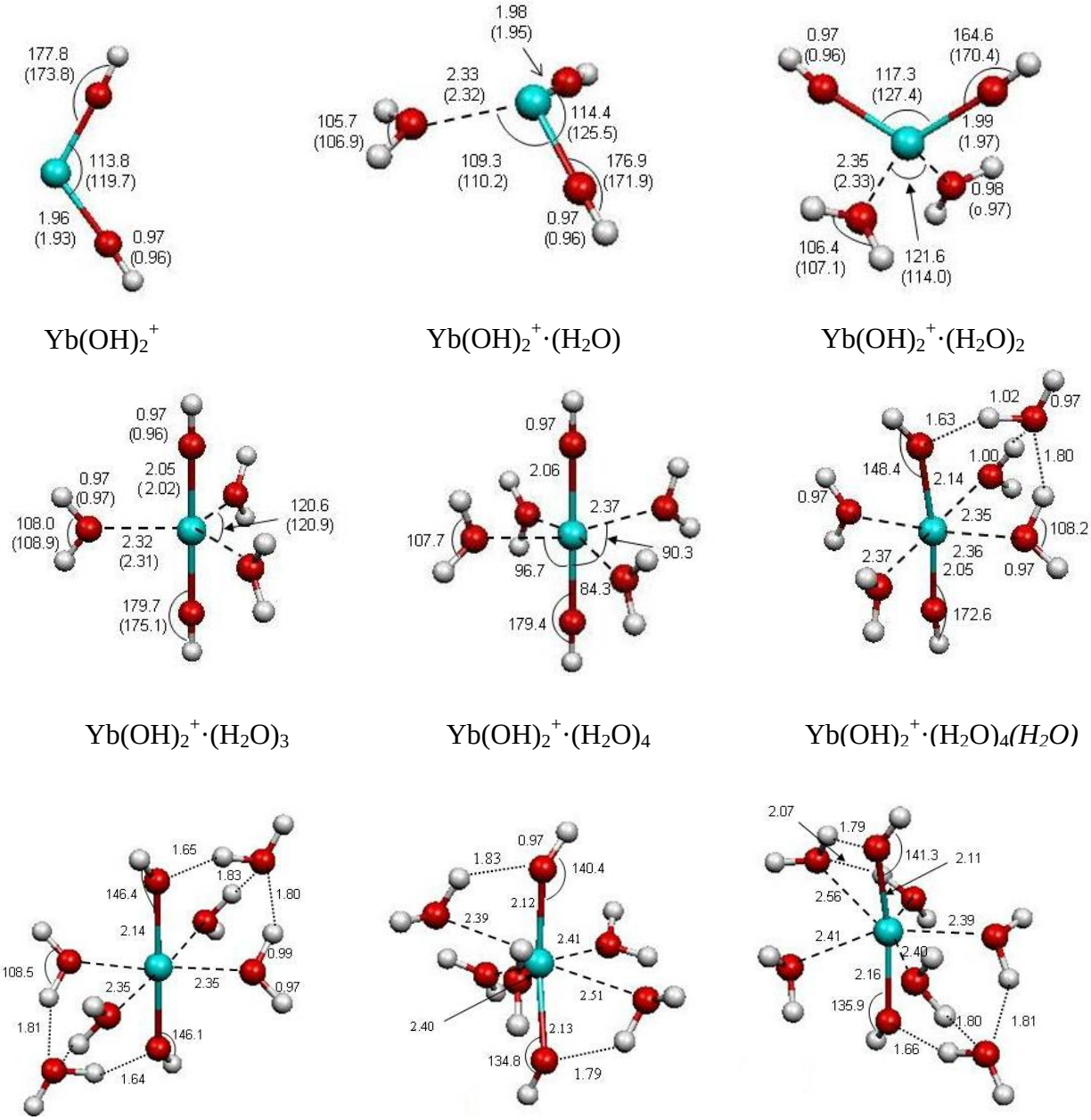

$Yb(OH)_2^+$ $Yb(OH)_2^+\cdot(H_2O)$ $Yb(OH)_2^+\cdot(H_2O)_2$

$Yb(OH)_2^+\cdot(H_2O)_3$ $Yb(OH)_2^+\cdot(H_2O)_4$ $Yb(OH)_2^+\cdot(H_2O)_4$*(H₂O)*

$Yb(OH)_2^+\cdot(H_2O)_4$*(H₂O)₂* $Yb(OH)_2^+\cdot(H_2O)_5$ $Yb(OH)_2^+\cdot(H_2O)_5$*(H₂O)*

Figure 9. Lowest energy equilibrium structures for $Yb(OH)_2^+\cdot(H_2O)_n$, n = 0-6. Distances (Å) and angles (degrees) are given. B3LYP/SDD-ANO results are in parentheses. $Yb(OH)_2^+\cdot(H_2O)_5$ and $Yb(OH)_2^+\cdot(H_2O)_5$*(H₂O)*, are high energy species. The relative energies of these latter species with respect to the ground state structures, $Yb(OH)_2^+\cdot(H_2O)_4$*(H₂O)* and $Yb(OH)_2^+\cdot(H_2O)_4$*(H₂O)₂*, respectively, are both 20 $kJ\cdot mol^{-1}$. Italics denote water molecules in the second solvation shell.

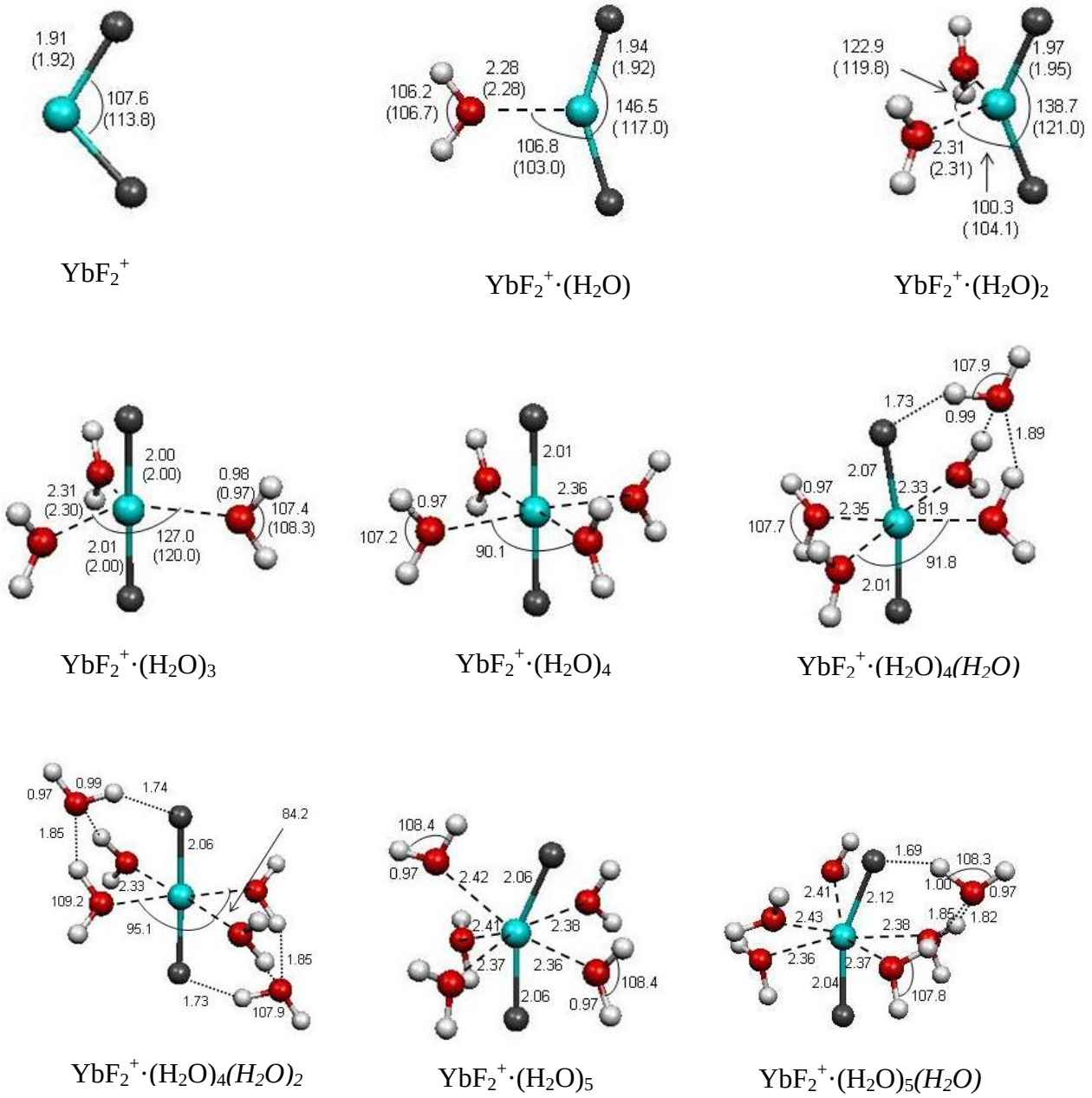

Figure 10. Lowest energy equilibrium structures for $YbF_2^+\cdot(H_2O)_n$, n = 0-6. Distances (Å) and angles (degrees) are given. B3LYP/SDD-ANO results are in parentheses. $YbF_2^+\cdot(H_2O)_5$ and $YbF_2^+\cdot(H_2O)_5$*(H₂O)*, are high energy species. The relative energies of these latter species with respect to the ground state structures, $YbF_2^+\cdot(H_2O)_4$*(H₂O)* and $YbF_2^+\cdot(H_2O)_4$*(H₂O)₂*, respectively, are 5 and 16 kJ·mol^{-1}. Italics denote water molecules in the second solvation shell.

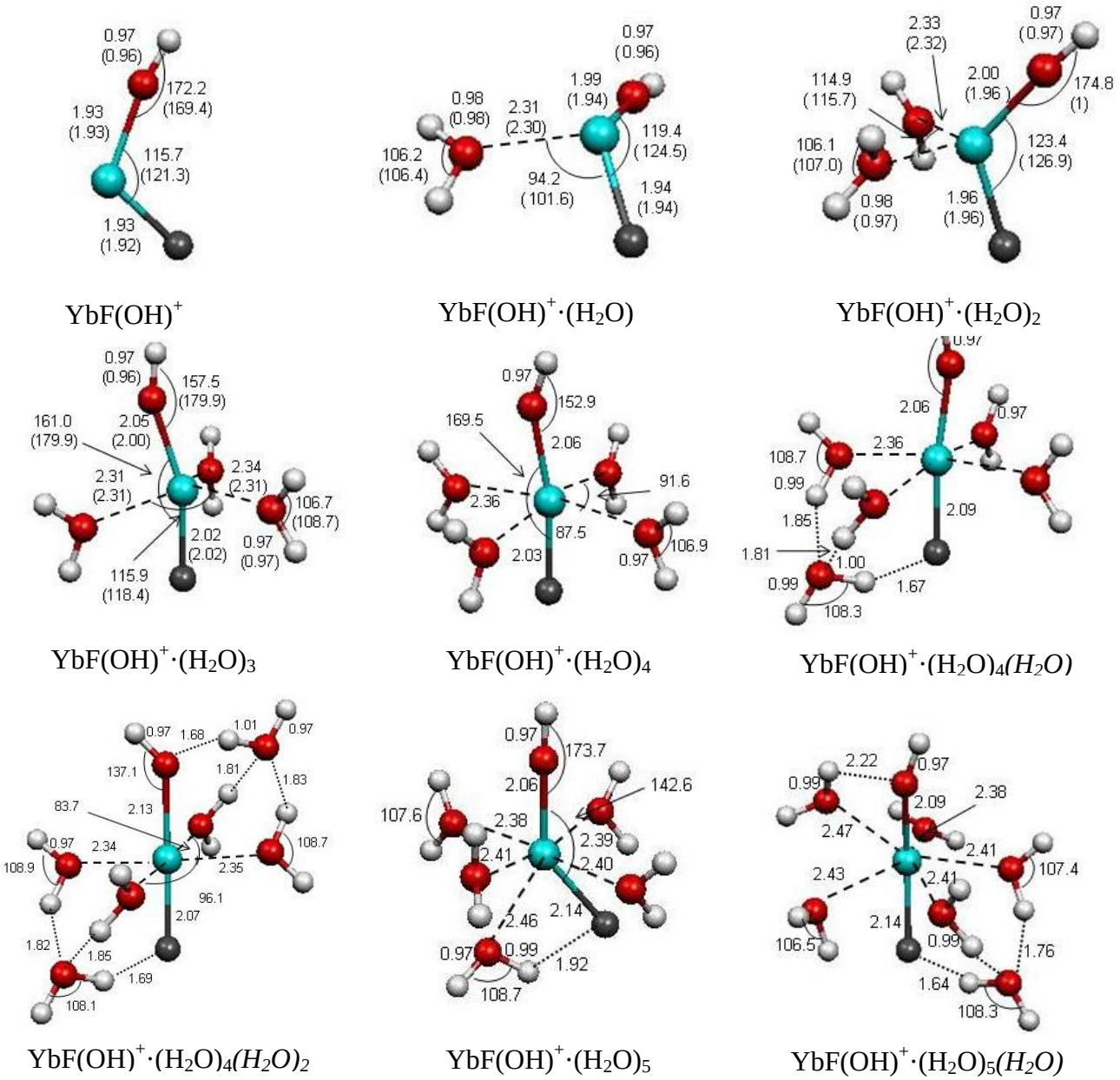

Figure 11. Lowest energy equilibrium structures for $YbF(OH)^{+}\cdot(H_2O)_n$, n = 0-6. Distances (Å) and angles (degrees) are given. B3LYP/SDD-ANO results are in parentheses. $YbF(OH)^{+}\cdot(H_2O)_5$ and $YbF(OH)^{+}\cdot(H_2O)_5$*(H_2O)*, are high energy species. The relative energies of these latter species with respect to the ground state structures, $YbF(OH)^{+}\cdot(H_2O)_4$*(H_2O)* and $YbF(OH)^{+}\cdot(H_2O)_4$*(H_2O)$_2$*, respectively, are 7 and 14 $kJ\cdot mol^{-1}$. Italics denote water molecules in the second solvation shell.

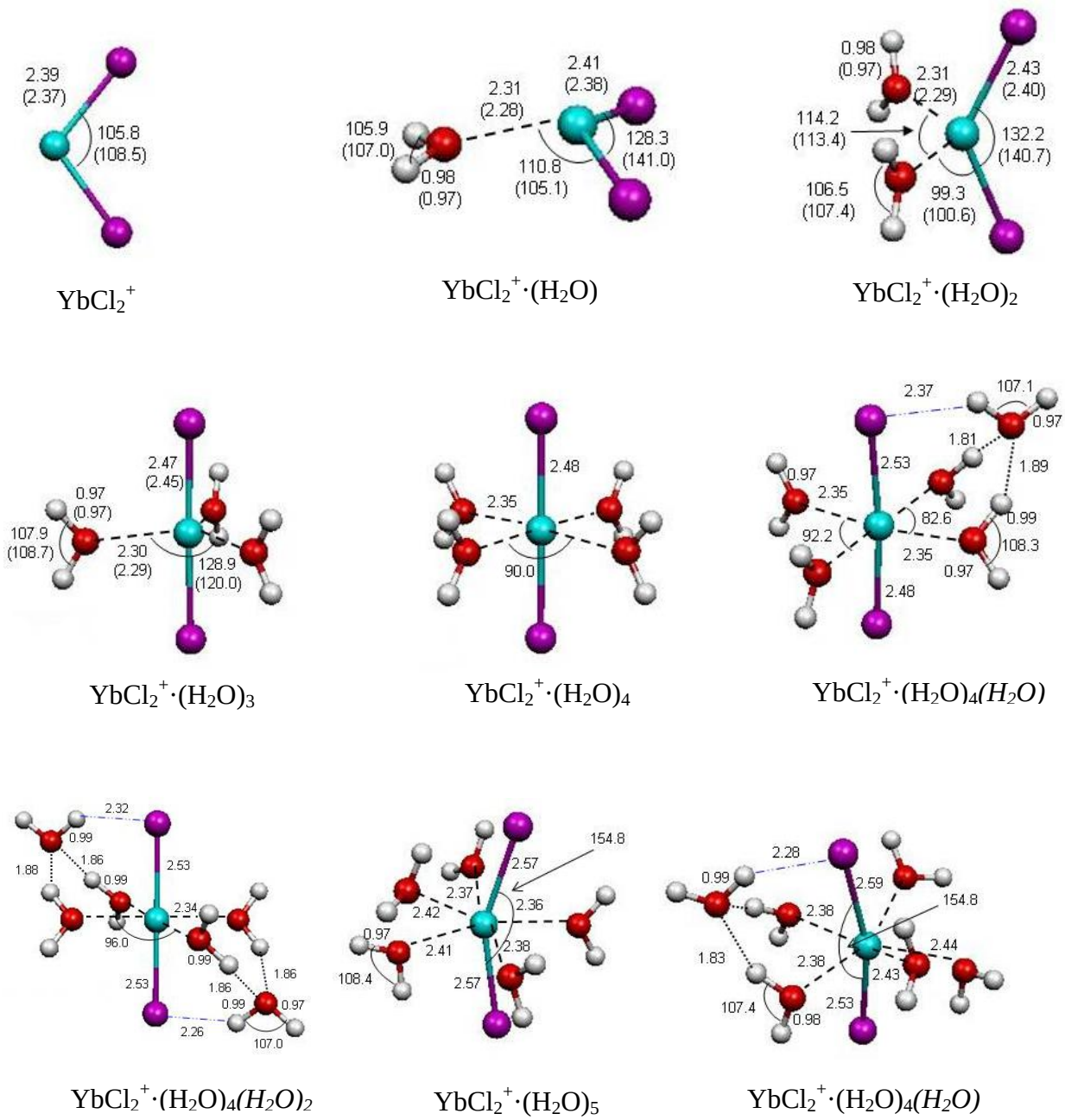

Figure 12. Lowest energy equilibrium structures for $YbCl_2^+\cdot(H_2O)_n$, n = 0-6. Distances (Å) and angles (degrees) are given. B3LYP/SDD-ANO results are in parentheses. $YbCl_2^+\cdot(H_2O)_5$ and $YbCl_2^+\cdot(H_2O)_5$*(H₂O)*, are high energy species. The relative energies of these latter species with respect to the ground state structures, $YbCl_2^+\cdot(H_2O)_4$*(H₂O)* and $YbCl_2^+\cdot(H_2O)_4$*(H₂O)₂*, respectively, are both 3 $kJ\cdot mol^{-1}$. Italics denote water molecules in the second solvation shell.

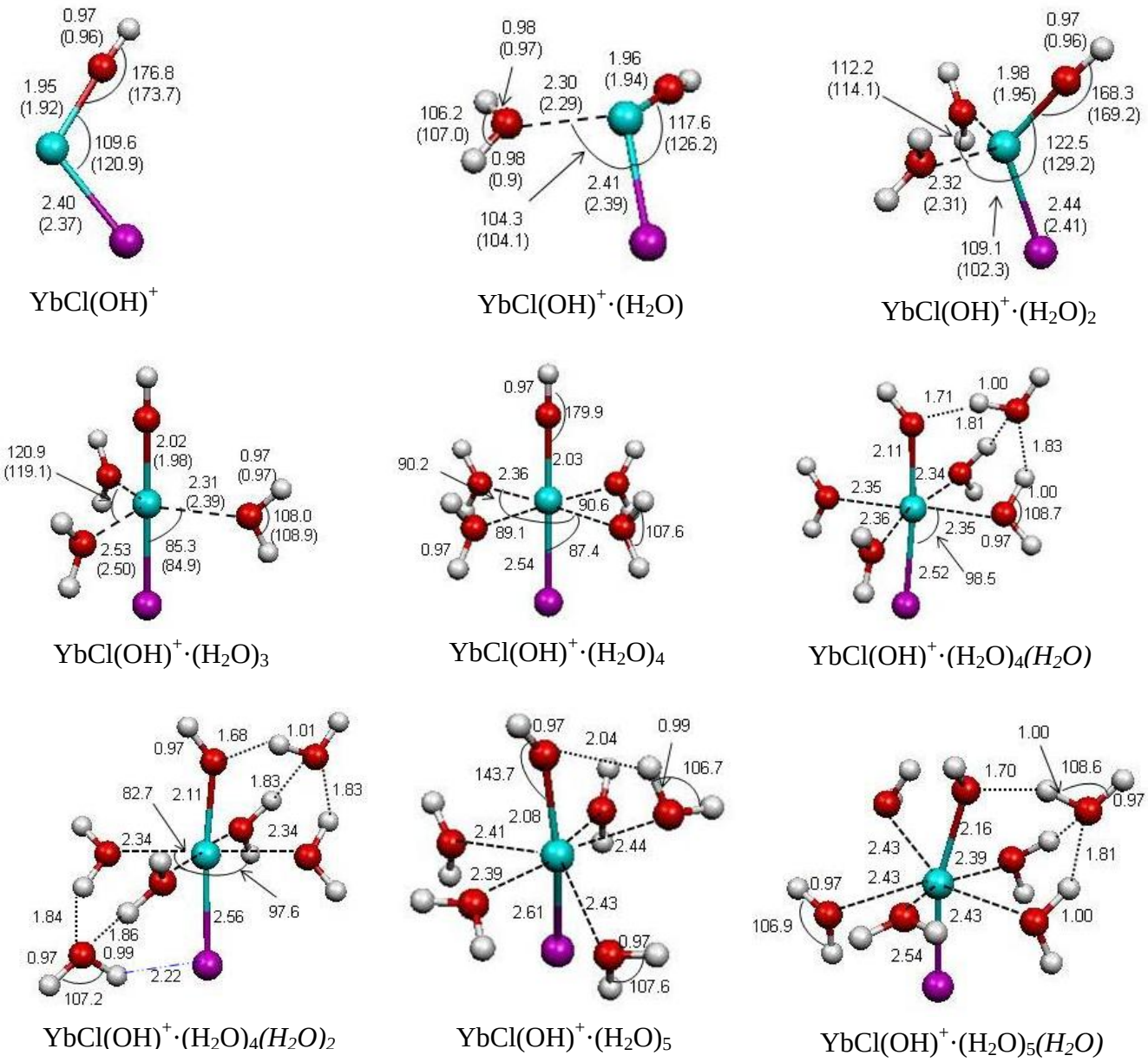

Figure 13. Lowest energy equilibrium structures for $YbCl(OH)^{+}\cdot(H_2O)_n$, n=0-6. Distances (Å) and angles (degrees) are given. B3LYP/SDD-ANO results are in parentheses. $YbCl(OH)^{+}\cdot(H_2O)_5$ and $YbCl(OH)^{+}\cdot(H_2O)_5$*(H₂O)*, are high energy species. The relative energies of these latter species with respect to the ground state structures, $YbCl(OH)^{+}\cdot(H_2O)_4$*(H₂O)* and $YbCl(OH)^{+}\cdot(H_2O)_4$*(H₂O)₂*, respectively, are 17 and 6 $kJ\cdot mol^{-1}$. Italics denote water molecules in the second solvation shell.

Table 1. YbX_2^+ and $YbX(OH)^+$ Hydration Kinetics Determined from Isolated Species Created by ESI-MS.[1]

Hydration Step	$Yb(OH)_2^+$	$YbCl(OH)^+$	$YbBr_2^+$	$YbBr(OH)^+$	YbI_2^+	$YbI(OH)^+$
$Z^+ + H_2O \rightarrow Z^+\cdot(H_2O)$	7.2 (28)	10.8 (42)		2.7 (10)		11 (42)
$Z^+\cdot(H_2O) + H_2O \rightarrow Z^+\cdot(H_2O)_2$	26 (100)	20 (77) [2]	16 (62)	20 (77)		17 (65)
$Z^+\cdot(H_2O)_2 + H_2O \rightarrow Z^+\cdot(H_2O)_3$	7.0 (27)		14 (54)	10 (38)	11 (42)	9.3 (36)
$Z^+\cdot(H_2O)_3 + H_2O \rightarrow Z^+\cdot(H_2O)_4$			12 (46)	4.2 (16)	9.5 (37)	4.6 (18)

[1] Values are reported in s^{-1}. Values in parentheses are percentages of the reaction rates normalized to the fastest hydration, the second hydration of $Yb(OH)_2^+$ and $Tm(OH)_2^+$. As discussed in the Experimental Section, all studied ions were thermalized. [2] This relative rate has an inordinately large uncertainty, approximately a factor of two, primarily due to a very low signal intensity.

Table 2. Tm and Yb Hydration Kinetics Determined from Isolated Species Created by ESI-MS.[1]

Hydration Step	$Tm(OH)_2^+$	$Yb(OH)_2^+$	$TmCl(OH)^+$	$YbCl(OH)^+$
$Z^+ + H_2O \rightarrow Z^+\cdot(H_2O)$	7.9 (31)	7.2 (28)	9.9 (38)	10.8 (42)
$Z^+\cdot(H_2O) + H_2O \rightarrow Z^+\cdot(H_2O)_2$	26 (100)	26 (100)	21 (81) [2]	20 (77) [3]
$Z^+\cdot(H_2O)_2 + H_2O \rightarrow Z^+\cdot(H_2O)_3$	6.4 (25)	7.0 (27)	13 (50)	
$Z^+\cdot(H_2O)_3 + H_2O \rightarrow Z^+\cdot(H_2O)_4$	0.062 (0.24)			

[1] Values are reported in s^{-1}. Values in parentheses are percentages of the reaction rates normalized to the fastest hydration, the second hydration of $Yb(OH)_2^+$ and $Tm(OH)_2^+$. As discussed in the Experimental Section, all studied ions were thermalized. [2] This relative rate has a large uncertainty, approximately ±50%, due to experimental limitations. [3] This relative rate has an inordinately large uncertainty, approximately a factor of two, primarily due to a very low signal intensity.

Table 3. Hydrolysis Kinetics for Isolated Species Produced by ESI.[1]

Isolated Ion	Hydrolysis Reaction	k
$YbCl(OH)^+$	$YbCl(OH)^+ + H_2O \rightarrow Yb(OH)_2^+ + HCl$	3.2
$YbCl(OH)^+\cdot(H_2O)$	$YbCl(OH)^+\cdot(H_2O) + H_2O \rightarrow Yb(OH)_2^+\cdot(H_2O) + HCl$	3.9
$TmCl(OH)^+$	$TmCl(OH)^+ + H_2O \rightarrow Tm(OH)_2^+ + HCl$	1.0
$TmCl(OH)^+\cdot(H_2O)$	$TmCl(OH)^+\cdot(H_2O) + H_2O \rightarrow Tm(OH)_2^+\cdot(H_2O) + HCl$	3.3
$TmCl(OH)^+\cdot(H_2O)_2$	$TmCl(OH)^+\cdot(H_2O)_2 + H_2O \rightarrow Tm(OH)_2^+\cdot(H_2O)_2 + HCl$	1.1
$YbBr_2^+\cdot(H_2O)$	$YbBr_2^+\cdot(H_2O) + H_2O \rightarrow YbBr(OH)^+\cdot(H_2O) + HBr$	1.1
$YbBr_2^+\cdot(H_2O)_2$	$YbBr_2^+\cdot(H_2O)_2 + H_2O \rightarrow YbBr(OH)^+\cdot(H_2O)_2 + HBr$	0.054
$YbBr(OH)^+$	$YbBr(OH)^+ + H_2O \rightarrow Yb(OH)_2^+ + HBr$	0.36
$YbI_2^+\cdot(H_2O)_2$	$YbI_2^+\cdot(H_2O)_2 + H_2O \rightarrow YbI(OH)^+\cdot(H_2O)_2 + HI$	0.87
$YbI(OH)^+$	$YbI(OH)^+ + H_2O \rightarrow Yb(OH)_2^+ + HI$	0.44
$YbI(OH)^+\cdot(H_2O)$	$YbI(OH)^+\cdot(H_2O) + H_2O \rightarrow Yb(OH)_2^+\cdot(H_2O) + HI$	0.084

[1] Rate values are reported in s^{-1} at constant water pressure (~10^{-6} Torr).

Table 4. Energy, Enthalpy, Entropy, and Gibbs Free Energy Changes for the Hydration Reactions at the PBE−ZORA/TZP and the B3LYP/SDD−ANO Levels of Theory.[1]

Reaction	$Yb(OH)_2^+$	$YbCl_2^+$	$YbCl(OH)^+$	YbF_2^+	$YbF(OH)^+$
n=1					
ΔE^0	-132 (-157)	-146 (-185)	-135 (-170)	-165 (-186)	-148 (-170)
ΔH^{298}	-133 (-159)	-147 (-188)	-137 (-172)	-175 (-188)	-148 (-172)
ΔS^{298}	-123 (-119)	-113 (-114)	-136 (-123)	-126 (-124)	-117 (-123)
ΔG^{298}	-96 (-124)	-113 (-154)	-96 (-135)	-137 (-151)	-113 (-135)
n=2					
ΔE^0	-130 (-143)	-139 (-163)	-129 (-155)	-144 (-165)	-128 (-153)
ΔH^{298}	-128 (-144)	-140 (-165)	-130 (-156)	-145 (-167)	-129 (-157)
ΔS^{298}	-100 (-117)	-132 (-135)	-129 (-127)	-125 (-121)	-124 (-122)
ΔG^{298}	-98 (-109)	-101 (-125)	-92 (-118)	-108 (-131)	-92 (-121)
n=3					
ΔE^0	-71 (-93)	-114 (-139)	-93 (-116)	-119 (-126)	-89 (-111)
ΔH^{298}	-75 (-96)	-116 (-143)	-95 (-119)	-121 (-129)	-92 (-111)
ΔS^{298}	-156 (-145)	-131 (-145)	-131 (-142)	-126 (-132)	-151 (-136)
ΔG^{298}	-29 (-53)	-77 (-100)	-56 (-77)	-84 (-90)	-47 (-70)
n=4					
ΔE^0	-75	-86	-86	-83	-78
ΔH^{298}	-74	-85	-85	-83	-77
ΔS^{298}	-115	-124	-121	-122	-112
ΔG^{298}	-39	-48	-49	-47	-44
n=5					
ΔE^0	-65	-60	-70	-65	-64
ΔH^{298}	-72	-65	-77	-71	-71
ΔS^{298}	-180	-154	-178	-170	-172
ΔG^{298}	-18	-19	-24	-24	-20
n=5*					
ΔE^0	-39	-57	-53	-60	-58
ΔH^{298}	-45	-62	-55	-64	-61
ΔS^{298}	-169	-164	-145	-155	-148
ΔG^{298}	5	-13	-12	-18	-17
n=6					
ΔE^0	-62	-52	-49	-61	-63
ΔH^{298}	-68	-60	-56	-66	-70
ΔS^{298}	-171	-164	-181	-165	-174
ΔG^{298}	-17	-11	-6	-17	-18

[1] The B3LYP/SDD–ANO level of theory is represented in parentheses. ΔE^0, ΔG^{298}, and ΔH^{298} are in $kJ \cdot mol^{-1}$ and ΔS^{298} is in $J \cdot K^{-1} \cdot mol^{-1}$. The reactions correspond to successive hydrations: $YbX_2^+ \cdot (H_2O)_{n-1} + H_2O \rightarrow YbX_2^+ \cdot (H_2O)_n$ or $YbX(OH)^+ \cdot (H_2O)_{n-1} + H_2O \rightarrow YbX(OH)^+ \cdot (H_2O)_n$. All of the reactants and products are in their ground state, therefore, the fifth and sixth water molecules are in the second coordination sphere. However, the pentahydrate complexes with five inner-sphere water molecules are included for comparison and are denoted as n=5*.

Table 5. $Yb(OH)_2^+$ and $YbCl(OH)^+$ Stretching Frequencies Computed at the PBE-ZORA/TZP and B3LYP/SDD-ANO Levels of Theory.[1]

Stretch	$Yb(OH)_2^+$	$YbCl(OH)^+$
Yb–O	696 (688) symmetric 662 (676) asymmetric	587 (680)
Yb–Cl	–	302 (362)
O–H	3769 (3908) symmetric 3758 (3902) asymmetric	3756 (3877)

[1] The B3LYP/SDD–ANO level of theory is represented in parentheses. Stretching frequencies are given in cm^{-1}.

References

1. Habenschuss A, Spedding FH (1979). J Chem Phys 70:2797-2806
2. Habenschuss A, Spedding FH (1979). J Chem Phys 70:3758-3763
3. Habenschuss A, Spedding FH (1980). J Chem Phys 73:442-450
4. Beudert R, Bertagnolli H, Zeller M (1997). J Chem Phys 106:8841-8848
5. Yaita T, Ito D, Tachimori S (1998). J Phys Chem B 102:3886-3891
6. Biggin S, Enderby JE, Hahn RL, Narten AH (1984). J Phys Chem 88:3634-3638
7. Annis BK, Hahn RL, Narten AH (1985). J Chem Phys 82:2086-2091
8. Steele ML, Wertz DL (1976). J Am Chem Soc 98:4424-4428
9. Steele ML, Wertz DL (1977). Inorg Chem 16:1225-1228
10. Johansson G, Yokoyama H (1990). Inorg Chem 29:2460-2466
11. Duvail M, Spezia R, Vitorge P (2008). Chem Phys Chem 9:693-696
12. Villa A, Hess B, Saint-Martin H (2009). J Phys Chem B 113:7270-7281
13. Chaussedent S, Monteil A (1996). J Chem Phys 105:6532-6537
14. Floris FM, Tani A (2001). J Chem Phys 115:4750-4765
15. Hughes SR, Nguyen T-N, Capobianco JA, Peslherbe GH (2005). Int J Mass Spectrom 241:283-294
16. Kuta J, Clark AE (2010). Inorg Chem 49:7808-7817
17. Buzko V, Sukhno I, Buzko M (2007). Int J Quantum Chem 107:2353-2360
18. Dinescu A, Clark AE (2008). J Phys Chem A 112:11198-11206
19. Clavaguéra C, Dognon J-P, Pyykkö P (2006). Chem Phys Lett 429:8-12
20. Lottermoser BG (1992). Ore Geol Rev 7:25-41
21. Migdisov AA, Williams-Jones AE, Wagner T (2009). Geochim Cosmochim Ac 73:7087-7109
22. Mayanovic RA, Jayanetti S, Anderson AJ, Bassett WA, Chou I-M (2002). J Phys Chem A 106:6591-6599
23. Mayanovic RA, Anderson AJ, Bassett WA, Chou I-M (2007). Chem Geol 239:266-283
24. Mayanovic RA, Anderson AJ, Bassett WA, Chou I-M (2009). Chem Geol 259:30-38
25. Gronert S (1998). J Am Soc Mass Spectrom 9:845-848
26. Van Stipdonk MJ, Chien W, Bulleigh K, Wu Q, Groenewold GS (2006). J Phys Chem A 110:959-970
27. Su T, Chesnavich WJ (1982). J Chem Phys 76:5183-5185
28. Perdew JP, Burke K, Ernzerhof M (1996). Phys Rev Lett 77:3865-3868
29. Perdew JP, Burke K, Ernzerhof M (1997). Phys Rev Lett 78:1396
30. ADF2004.01 SCM; Theoretical Chemistry, V. U., Amsterdam, The Netherlands, http://www.scm.com.
31. Fonseca Guerra C, Snijders JG, te Velde G, Baerends EJ (1998). Theor Chem Acc 99:391-403
32. te Velde G, Bickelhaupt FM, van Gisbergen SJA, Fonseca Guerra C, Baerends EJ, Snijders JG, Ziegler T (2001). J Comput Chem 22:931-967
33. Becke AD (1993). J Chem Phys 98:5648-5652
34. Lee CT, Yang WT, Parr RG (1988). Phys Rev B 37:785-789
35. Dolg M, Stoll H, Preuss H (1989). Journal of Chemical Physics 90 (3):1730-1734
36. Cao XY, Dolg M (2001). J Chem Phys 115:7348-7355
37. Cao XY, Dolg M (2002). Journal of Molecular Structure-Theochem 581:139-147
38. Krishnan R, Binkley JS, Seeger R, Pople JA (1980). J Chem Phys 72:650-654
39. Blaudeau JP, McGrath MP, Curtiss LA, Radom L (1997). J Chem Phys 107:5016-5021
40. Clark T, Chandrasekhar J, Spitznagel GW, Schleyer PV (1983). J Comput Chem 4:294-301
41. Gaussian 03 Revision C02; Frisch, M. J.; et al. See Supporting Information for full citation.
42. Michelini MD, Marcalo J, Russo N, Gibson JK (2010). Inorganic Chemistry 49 (8):3836-3850
43. Reed AE, Weinstock RB, Weinhold F (1985). J Chem Phys 83:735-746
44. Bader RFW (1990) Atoms in Molecules. A Quantum Theory. Oxford University Press, Oxford
45. Varetto, U.; Molekel 4.3 ed. Manno, Switzerland.

46. Cheng P, Koyanagi GK, Bohme DK (2006). Chem Phys Chem 7:1813-1819
47. Cheng P, Koyanagi GK, Bohme DK (2007). J Phys Chem A 111:8561-8573
48. Milburn RK, Baranov VI, Hopkinson AC, Bohme DK (1998). J Phys Chem A 102:9803-9810
49. Shoeib T, Milburn RK, Koyanagi GK, Lavrov VV, Bohme DK, Siu KWM, Hopkinson AC (2000). Int J Mass Spectrom 201:87-100
50. Anbalagan V, Chien W, Gresham GL, Groenewold GS, Van Stipdonk MJ (2004). Rapid Commun Mass Spectrom 18:3028-3034
51. Irikura KK (1999). J Am Chem Soc 121:7689-7695

LEGAL DISCLAIMER

This document was prepared as an account of work sponsored by the United States Government. While this document is believed to contain correct information, neither the United States Government nor any agency thereof, nor The Regents of the University of California, nor any of their employees, makes any warranty, express or implied, or assumes any legal responsibility for the accuracy, completeness, or usefulness of any information, apparatus, product, or process disclosed, or represents that its use would not infringe privately owned rights. Reference herein to any specific commercial product, process, or service by its trade name, trademark, manufacturer, or otherwise, does not necessarily constitute or imply its endorsement, recommendation, or favoring by the United States Government or any agency thereof, or The Regents of the University of California. The views and opinions of authors expressed herein do not necessarily state or reflect those of the United States Government or any agency thereof or The Regents of the University of California.